

6 April 2018

Response to Dr George Kiladis (Reviewer 1) comments on

“Multivariate analysis of Kelvin wave seasonal variability in ECMWF L91 analyses”

by Marten Blaauw and Nedjeljka Žagar

Dear Dr Kiladis,

Thank you very much for your detailed and constructive comments on the paper.

We have taken them into account in the revised paper.

We hope that the revised paper better highlights analysis possibilities offered by the MODES package i.e. by the multivariate analysis of the Kelvin wave and other equatorial waves on the sphere.

Enclosed please find our responses to your comments using the same organisation as in the review. Your comments are coloured blue whereas our responses are in black.

Yours sincerely,

Marten Blaauw and Nedjeljka Žagar

GENERAL COMMENT:

This is a fine paper on Kelvin activity that utilizes the normal mode function decomposition method pioneered by Kasahara and Puri and further refined by Zagar and others. The paper essentially represents a “proof of concept” of the technique as applied to Kelvin waves, although a lot of interesting information is included. The paper succeeds in demonstrating the utility of NMF decomposition and should provide a good starting point for those interesting in pursuing this approach, especially given the fact that software has been conveniently set up for others to apply as described in Zagar et al. 2015.

SPECIFIC COMMENTS:

The paper appears to be in good shape overall, although there are some lingering questions in this reviewer’s mind about interpretation, as discussed below. This mainly has to do with lumping all of the vertical modes together, which does not necessarily seem physical to me for all the cases considered. Perhaps not for this study, but it would be very instructive and add a lot of value to come up with some associated relationships between the subseasonal variability in Kelvin energy discussed here and some indices of tropical convection. The authors have made an initial attempt of this for the seasonal cycle and interannual timescale and their interpretation seems reasonable there. As far as higher frequencies go, for instance, cross spectra between the timeseries shown in Fig. 5 and geographically distributed OLR or brightness temperature could be very revealing. Ultimately, this could also be done for other modes isolated by this technique too. Figure captions could be improved overall, especially at the locations noted below. Also the text is not as clear as it could be in places.

Response: Thank you very much for the comments and suggestions. Indeed, the first goal of the paper is to introduce a novel methodology to analyze linear Kelvin waves on the sphere. As shown by Boyd and Zhou (J. Atmos. Sci., 2008), the degree of the Kelvin wave equatorial confinement on the sphere is controlled not only by the equivalent depth (i.e. by the equatorial Rossby radius of deformation) as on the equatorial beta plane but also by the zonal wavenumber. Therefore, even barotropic Kelvin waves with equivalent depth around 10 km are on the sphere trapped to the equator. This is a strong reason to use the spherical Kelvin wave solution for the projection.

We demonstrate the method by examples and diagnostics of seasonal variability that leads to results that are in agreement with previous studies, but also provide new understanding. As the first paper using this method for the Kelvin wave analysis, it takes space to present how the modal decomposition works and what kind of outputs it provides. As you pointed out, there are numerous research questions where this method may add insight and complement existing diagnostics. We find it hard to expand the paper beyond what has been already included. One of the topics left for future work is the suggested cross spectra.

Technical corrections

32: do you mean “modulate the TTL”?

Response: Yes. Corrected.

49: nomenclature here is slightly confusing: hkw has not been defined. If you are indeed following Holton then this is a perturbation term, otherwise it might be mistaken for the equivalent depth.

Response: The paragraph has been reformulated. We clarify that h_{kw} is the geopotential height perturbation associated with the Kelvin wave.

58: this statement is misleading, actually the tropical “cloud activity” really refers to the mean cloudiness (Tindall et al. were citing Zhang 1993) which is a maximum in January and minimum in July near the equator.

Response: The sentence has been changed as follows:

Such analysis was carried out by \cite{Tindall2006b} for the lower stratosphere for the ERA-15 data in 1981-93 period. Their results suggested that KWs contributes approximately 1 K² of the temperature variance on the equator with peak activity occurring during solstice seasons at 100 hPa, during December-February at 70 hPa and at 50 hPa it occurs during the easterly to westerly quasi-biennial oscillation (QBO) phase transition.

79: the horizontal and temporal resolution from line 106 should also be included here.

Response: Changed as suggested.

93: not sure what “denotdm” means here, should this be in parentheses (denoted m)?

Response: We are sorry for the typo. It has been corrected.

126: I am confused by one aspect of this procedure: As nicely discussed in detail by Zagar et al. (2015) and references therein, each vertical mode is characterized by an equivalent depth and associated horizontal structure function. Here it appears that all of the vertical modes are summed. For the sake of discussion, suppose we have a stratospheric “free” Kelvin mode which is present at the same time as an independent “convectively coupled” Kelvin mode that has maximum amplitude in the troposphere. These could be either collocated in lat-lon space or present at the same time in different regions of the globe. I think it would be profitable to make clear that it would still be possible to separate these modes by this procedure if one had enough additional information on the associated equivalent depths of each mode, which could be much different from each other. Stratospheric Kelvin waves at 50hPa follow dispersion related to a 120 m equivalent, whereas this is more like 25 m for convectively coupled waves. Acknowledging this fact seems appropriate, along with perhaps some words on how it could be dealt with in practice. I wonder, for instance, if investigating time series of KW energy for individual vertical modes could be done in a systematic way, using an extension of the approach in Zagar and Franzke (2015)? I think it would add considerable value to add a short discussion on these points.

Response: We deliberately use all vertical modes summed up their sum provides the total Kelvin wave signal in physical space. We do use a smaller number of vertical

modes ($M=60$) then the number of levels with data (91) but the decomposition provides the complete information about the waves in the studied layer of upper troposphere and above. Because the majority of the results concerns the total KW signal in physical space we do not make specific references to equivalent depths in the discussion.

In the revised paper, we add some more discussion about the role of equivalent depth in the construction process of the projection. It is not straightforward to discuss results on any level in terms of equivalent depths as for this we would need information on the amount of the Kelvin wave signal projecting to various equivalent depths. This can be obtained by filtering to physical space each vertical mode separately that increases the computational demand by factor m . In this study we limited the discussion to the basic concept of the method and seasonal features of the complete Kelvin wave signal.

It would be possible to split the Kelvin wave filtering in terms of vertical modes and discuss how (if) the KW signal in terms of m is grouped in various ranges of m (as indicated for MJO-related variance in Žagar and Franzke (GRL, 2015)). Such diagnosis is less trivial in the case with the high model lid such as here (1 Pa). The top model levels in this period also had some artificial damping and wave reflections. One way to solve this would be to limit the NMF projection to the troposphere only or the troposphere+lower stratosphere as for example done by Žagar et al (2017, JAS) using the ERA Interim data. The ongoing work on the KW properties in reanalysis datasets should provide further insight which we hope to report soon.

137: As in the previous comment, you are including the projection onto the vertical mode that corresponds to, say, the 10 km equivalent depth, which I would assume be more representative of an external Kelvin mode. Perhaps one way to look at this is to assume that there would be a “spectrum” of vertical modes for each situation depending on how much the data projects onto each individual mode. I think it would be worth elaborating on this point here, especially for those who may be less familiar with the idea that you are discretizing the vertical and associated horizontal structures for a reason, but that in reality a given atmospheric disturbance will be composed of a potentially different combination of these from case to case.

Response: The revised paper includes some more discussion of the role of vertical decomposition i.e. the equivalent depth. We do not filter any vertical mode separately as it would broaden presentation beyond the scope of this paper. Earlier paper by Žagar et al (Mon. Wea. Rev., 2009b) showed that presentation in terms of vertical modes in time can be very useful to represent the vertical Kelvin wave propagation. It is another topic left for future studies.

Our preliminary results on how the KW energy projects indeed among a “spectrum” of vertical modes, divides the vertical modes into roughly two groups: the vertical modes with equivalent depths ranging from 10 to 0.1 km that represent a part of the signal characterized by a strong (semi)annual periodicity. The second group contains signal that project to waves with equivalent depths ranging from 100 to 10 m and are observed throughout the year. The physical signature of these waves, decomposed based on their numerically discretized vertical structure functions, is not well understood yet in relation to the free stratospheric and the convectively coupled KWs that you mentioned in the comment. As for the previous comment, a dataset with a lower lid such as reanalysis data would make the interpretation task easier.

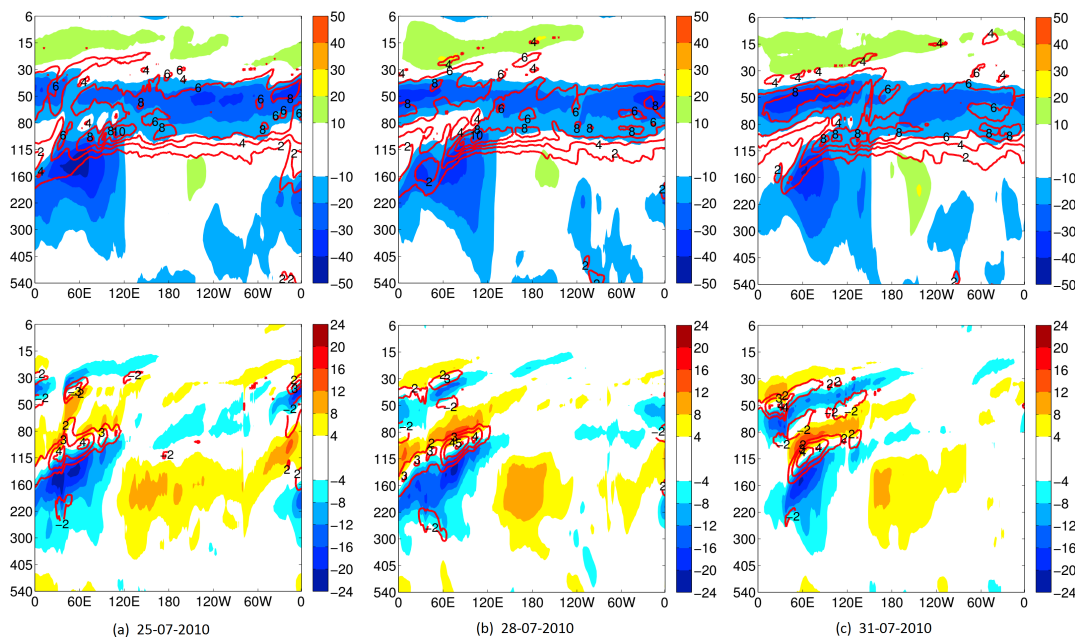
138: probably should describe the figure in more detail first, such as the tilted structures of what fields are shown, etc., before launching into the implications.

Response: We changed section 2.2 to provide more clarity on the Kelvin wave examples. In Fig. 2 different July days in 2010 have been chosen (25, 28, 31 July) with a shorter time interval of three days in order to visualize the stratospheric KW propagation more clearly. The chronological order of explanation has changed in section 2.2 such that Figures 1 and 2 are described in more detail first with respect to the free stratospheric waves as well as quasi-stationary tropopause structures, followed by the implications.

145: “strong KW activity was present” I guess you are referring to the case discussed in Fig. 2? Are you saying that the entire pattern shown represents a free Kelvin mode? This is where some information on the associated convective activity might be very useful.

Response: Yes. In Fig. 2 we refer in particular to 28 and 31 July when the wave package is located in the Eastern Hemisphere. It is hard to argue that the whole stratospheric pattern represents a free Kelvin mode. We rewritten the discussion. There are clear signs of eastward and downward KW propagation above 80 hPa. It is hard to see visually where coupled Kelvin modes in the TTL end and where the free Kelvin modes start to dominate.

To clarify the relationship between the observed Kelvin wave activity in relation to the background wind and stratification conditions, we illustrate below the background fields as well:



The bottom three panels are as in revised Fig. 2 in the paper. The top three panels illustrate from the ECMWF zonal wind (blue-to-red shades, for $|U| > 10 \text{ ms}^{-1}$) and the static stability (red contours, for $N^2 > 2 \times 10^{-4} \text{ s}^{-2}$) fields. The easterly winds in the TTL (160 hPa) create a “window” through which the Kelvin wave energy can “escape” into the stratosphere. A double-folding structure in the static stability fields (up to $8 \times 10^{-4} \text{ s}^{-2}$) coincides with large amplitude Kelvin wave temperature perturbations (up to 4 K).

154: Another very useful bit of information would relate the activity of KWs (such as measured by the energy spectrum) to the QBO, perhaps in a future study.

Response: We agree and the Kelvin wave-QBO relation is one of the couplings we hope to address using a longer time series of data from reanalyses.

161: “climatological zonal structure” at first, I thought this was only for the period of Fig. 2 and the figure caption does not help.

Response: The caption has been re-written. Figure 3 shows the six-year average of full zonal wind in the analyses and static stability.

191: “resonates” => “fluctuates” might be a better choice of words.

Response: Changed as suggested.

244: I’m unsure what the tidal effect would look like, but could the tide itself be projecting onto the Kelvin structure in some way? It doesn’t seem that a Kelvin wave structure should be impacted by the tide, especially if you consider that these are both orthogonal “normal modes”. This may deserve a few more words and could emphasize one potential drawback of the approach.

Response: Rewritten as “The spectrum contains a peak at 1-day period associated with the diurnal tide partially projecting on the Kelvin waves.” without further elaboration which is beyond the scope of present study. An unpublished master thesis used MODES to analyze what large-scale wave the tides in the same dataset project on.

259: Probably should use a bit more care when discussing the impact of the QBO since this is highly dependent on the level you are referring to. One way to put it might be to point out that vertical penetration of Kelvin wave energy into the stratosphere depends on the state of the QBO in the lower layers of the stratosphere.

Response: Corrected as: “Moreover, KW activity is enhanced whenever easterly QBO winds are present down into the lower stratosphere \citep{Baldwin2001, Alexander2010} or during El Niño \citep{Yang2013}.”

269: It turns out the the QBO was easterly at 50 hPa in July 2007, but only just beginning the easterly phase at that level.

Response: Thank you. We have added this comment.

291: What is the advantage of using “absolute amplitude” over say, variances? This should be discussed and justified.

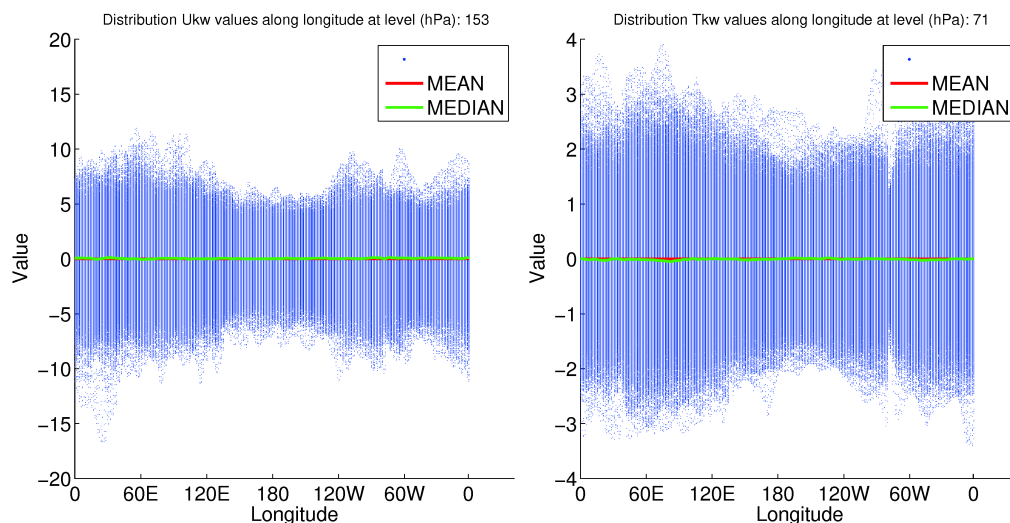
Response: The explanation has been added as the following footnote in the revised manuscript: “Most previous studies define KW activity as square amplitude rather than absolute amplitude. In our high resolution dataset we observe highly localized patterns of the KW activity in the Eastern hemisphere due to ongoing wave amplification. By using absolute amplitudes we better visualize the longitudinal structure of the KW activity in comparison to its local maxima.”

287: I wouldn't insist on it, but it may also be of interest to examine whether there is significant skewness in the distributions of the raw filtered data on the subseasonal timescales, and whether they are approximately normal. In other words, does it matter what the phase of the Kelvin component is at a given level, or are negative perturbations approximately the opposite of positive ones?

Response: To answer your question, we checked the distribution of raw filtered data with applied low-pass filter over periods of 3-20 days for the KW zonal wind and temperature components at several levels. Enclosed are examples for (left panel) KW zonal wind at ~153 hPa (in ms^{-1}) and (right panel) KW temperature at ~71 hPa (in K). All scatter point values over 6-year period are plotted as a function of longitude. The 6-year mean (red line) and median (green line) are computed for each longitude.

It follows that the distribution is well-described as normal on subseasonal timescales. Mean and median values are approximately zero.

The same applies for filtered data for periods 20-90 days and for other levels.



292: caption and discussion of Fig. 7 is confusing. When describing 7a the caption says "mean" when you really mean "(semi)annual" as discussed above. Isn't 7c for the high frequency? If so the caption should say so.

Response: Figure caption has been rewritten. The word "mean" has been removed. All three panels represented 6-year mean Kelvin wave zonal wind and temperature fields that are filtered over three different specific ranges of periods.

297: "quadrupole" is more commonly used, but perhaps not in Europe.

Response: Changed as suggested.

310: There is decent agreement between the results here and those of Flannaghan and Fueglistaler as to where the Kelvin activity is maximized and I think this should be discussed at this point as well as below (e.g. Fig. 6 of Flannaghan and Fueglistaler 2013).

Response: This is discussed in details in section 4.4 where seasonal decomposition similar to Figure 6 of Flannaghan and Fueglistaler (2013) is presented.

333: This is a very interesting analysis and the link between the low frequency Kelvin component to the “Gill-type response” is very insightful. However, the pure Gill response is only Kelvin-like to the east and includes Rossby gyres to the west of the heating, so at least part of the easterlies would not necessarily be due to a projection on Kelvin waves. This should at least be mentioned, if not discussed in more detail.

Response: The Gill-type response results from the steady-state, long-wave approximation without background wind that leads to an idealized view with Kelvin waves represented only by westerlies east of the Maritime continent. Real data is more complex and we have been more careful in the revised paper in using the “Gill-type KW” term following Salby and Garcia (1987). We emphasize that we discuss the low-frequency Kelvin wave response to large-scale tropical heating that has strong easterly zonal wind component as well.

356: This is a clever way of getting at the impact of the quasi-stationary Kelvin wave forcing.

Response: Thank you

384: It would indeed be interesting to see what the relationship between intraseasonal Kelvin activity isolated here might be to the convective activity on the same timescale.

Response: We recognize this as an interesting question but beyond the scope of the present paper.

416: It seems that the right panels refer to a specific longitude only but this is never identified in the text or caption.

Response: Figure caption has been re-written and discussion improved. The amplitude of the KW zonal wind wave are maximal amplitudes occurring anywhere along the equator averaged over the 6-year period for each calendar month.

431: Now it seems that these numbers are somehow zonal averages? Rather confusing, and once again the figure caption does not help either.

Response: Corrected. These numbers are maximal values found along the equator.

437: I guess this is not shown? That should be noted.

Response: Added as suggested.

6 April 2018

Response to the comments of Reviewer 2 on

“Multivariate analysis of Kelvin wave seasonal variability in ECMWF L91 analyses”

by Marten Blaauw and Nedjeljka Žagar

Dear Referee,

thank you very much for your comments and suggestion on our manuscript.

We have revised paper following your criticism and suggestions. In particular, we have re-written parts of Introduction and methodology sections in order to better describe novel features of the applied method.

Enclosed please find our responses to your comments using the same organisation as in your review. Your comments are coloured blue whereas our responses are in black.

Your sincerely,

Marten Blaauw and Nedjeljka Žagar

GENERAL COMMENTS:

The authors have developed a powerful analysis technique whereby they are able to decompose any 3-dimensional atmospheric analysis product into its (linear) global normal modes, which includes the equatorial Kelvin wave as one of its components. As I understand it, this decomposition is computed for each individual time point of the analysis, and no information on the propagation from one time point to the next is used for the categorization into the different normal modes. This is quite different to what has been done in many other studies, for example, Wheeler and Kiladis (1999) who used wavenumber-frequency spectra and filtering for identification of equatorial waves. Therefore, what is called a "Kelvin wave" in this study is somewhat different to those C1 ACPD Interactive comment Printer-friendly version Discussion paper other studies, since the identified structures may not be propagating, but may be stationary or even display propagation in the opposite direction to what is usually ascribed to a particular mode. This difference with other studies requires careful explanation and should be highlighted, but is not necessarily a problem with the paper.

Another aspect of this work that I think needs highlighting is that the normal mode decomposition is based on the assumption that the equations of motion are linearized about a basic state of rest (i.e. zero winds, line 88). It is unclear to me how much this assumption may affect the results.

I also wonder what assumptions are made about the static stability for the calculation of the normal modes. The static stability is important for setting the relationship between the horizontal and vertical structures of the normal modes. For the same gravity wave speed, c , a Kelvin wave in the stratosphere will have a shorter vertical wavelength than a Kelvin wave in the troposphere, due to the different static stability. But both these Kelvin waves will have the same meridional (horizontal) structure, which is set by the equatorial Rossby radius, a function of c , where c is the gravity wave speed. The meridional length scale is actually $\sqrt{c/\beta}$, where β is df/dy . So what temperature and static stability profiles do you assume, and how can this affect the results? What would happen if you assumed a "moist static stability" for the troposphere? Instead of the traditional dry static stability?

To be more convinced about the utility of the technique for understanding, I also wonder what the wavenumber-frequency spectra of the decomposed "Kelvin waves" would look like. You could do this at each level and see what equivalent depth dominates at each level. I imagine that in the troposphere you may see a predominance of the MJO and the $c \sim 20\text{m/s}$ convectively-coupled Kelvin waves, but as you enter the stratosphere the equivalent depth should start increasing due to the filtering provided by the background winds. These results would be useful to compare to Hendon and Wheeler (2008, J. Atmos. Sci., Vol 65).

Perhaps another interesting comparison to make is how the transient behaviour in OLR matches the transient behaviour in your Kelvin wave dataset. Do the convectively-coupled Kelvin waves identified in OLR by the technique of Wheeler and Kiladis (1999) show up in your independent Kelvin wave dataset? To me, this would be much more interesting than some of the analysis provided here.

In summary, I must admit that I was a little underwhelmed by the results presented here. I think more interesting things could have been studied. But at the same time, the work is rigorous and may be more interesting to others, so it still adds something to the published literature

Response

1. Methodology

The first goal of our paper is to introduce a novel methodology for the Kelvin wave filtering and demonstrate it by examples and diagnostics with similarity to previous studies.

We use analytical relationships for the horizontal structure of the Kelvin wave wind and geopotential height perturbations on the sphere. This is different from many previous studies which relied on the Kelvin wave solutions on the equatorial beta plane. We sum up linear Kelvin wave solutions in many shallow-water equation systems (60 in our case). The extension of the Kelvin wave analysis by 2D approach (on individual horizontal levels or vertical planes) to the three-dimensional (3D) spherical coordinates is an important step for realistic filtering of Kelvin waves in global datasets. As shown by Boyd and Zhou (J. Atmos. Sci., 2008), the degree of the Kelvin wave equatorial confinement on the sphere is controlled not only by the equivalent depth (i.e. by the equatorial Rossby radius of deformation) but also by the zonal wavenumber. Therefore, even barotropic Kelvin waves with equivalent depth around 10 km on the sphere are trapped to the equator. This is a strong reason to use the spherical Kelvin wave solution for the projection.

Data projection on horizontal Kelvin wave structure, along with other equatorial waves, on individual time instants was performed before by Tindall et al (2006, QJRMS). In the revised paper we add also a reference to a similar approach by Yang et al (J. Atmos. Sci., 2003) for data on individual levels using the equatorial beta plane solutions and using the equatorial Rossby deformation radius as the fitting parameter. We also refer to Žagar et al (QJRMS, 2005, 2007) who used analytical solutions on the equatorial beta plane to analyze the distribution of the equatorial wave variance in the short-term forecast errors of the ECWMF model.

Our Kelvin wave signal at any time is a sum of many Kelvin waves with different phase speeds. As the applied normal-mode function projection provides a complete projection basis, we can quantify the amount of total variance associated with Kelvin waves in global data.

We have re-written parts of Introduction and other sections in order to better highlight methodology approach and what kind of outputs it provides. We believe that here are many research questions regarding the Kelvin and other equatorial waves where the presented method can provide added insight and complement other methods.

2. Comparison with spectral space-time filtering (so-called Wheeler-Kiladis diagrams)

Our filtering procedure is different from the widely used spectral space-time filtering pioneering by Hayashi (1972) that applies Kelvin wave dispersion relations. We analyze circulation data at selected processing times independently of other times. In other words, the dispersion relationship for the linear Kelvin waves on the sphere, used to derive the analytical expressions for the Kelvin wave wind and geopotential height, is not used explicitly in the data analysis. At every analyzed time step, in every grid point we

sum up contributions from 60 Kelvin wave solutions for each zonal wavenumber. Nevertheless, the linear wave features readily persist in our outputs for the Kelvin waves as shown in the example and Hovmoeller diagrams in the Result section. This result alone is very interesting as it validates the linear wave theory approach that has been successfully employed in many studies, especially for the large-scale tropical circulation features.

The spectral space-time filtering does not consider the meridional wave structure. The normal-mode function projection, thanks to its 3D orthogonal structures, allows a full quantification of the Kelvin wave signal and its spatial localization.

We agree that would be interesting to combine the two different methods on analyzing Kelvin waves. But such analysis is beyond the scope of the present paper. Previously mentioned paper by Yang et al (J. Atmos. Sci., 2003) and several their follow-on studies combined the space-time filtering and the projection on analytical equatorial wave solution on the equatorial beta plane. Our 6.5 year long dataset is also shorter than time series used in space-time filtering. We aim to perform some comparison of the two methods within the ongoing analysis of Kelvin waves in several decades long time series from reanalysis data.

3. Linearization about a basic state of rest

This is not a drawback of the method as wave frequencies are used solely for the formulation of the projection basis and not for studying the wave propagation properties. Namely, the frequencies differ depending on whether the linearization is performed around the state of rest as in our case or the mean flow is taken into account. If the mean zonal flow is taken into account, the frequencies of wave solutions can become unstable, as well as continuous, except for a few of the lowest balanced modes (Kasahara, 1980). Fortunately, the meridional structures of the Hough functions are not significantly different if the linearization is performed around the non-zero mean zonal flow (see Corrigendum to Kasahara, 1980, J. Atmos. Sci.). It is therefore suitable to use the Hough functions constructed with reference to the basic state at rest as a basis for the projection.

We have discussed this issue in the paper by Žagar et al. (2015, Geo. Model Dev.) where the projection method has been described in details. In Žagar et al. (2017, J. Atmos. Sci.) we demonstrated that even inertia-gravity waves with smaller scales can be successfully represented by the method. Another paper using the same decomposition, currently also in ACP Discussion, demonstrates the same point: <https://www.atmos-chem-phys-discuss.net/acp-2018-228/>

The impact of latitudinal shear on the Kelvin waves was previously shown negligible by Boyd (1978, J. Atmos. Sci.).

4. Assumptions about the static stability for the calculation of the normal modes

Stability and temperature are globally averaged and their temporal changes are not significant for the structure of the basis functions for the projection. In any case, definition of stability is a part of the derivation procedure by Kasahara and Puri (1981, Mon. Wea. Rev.) that considers hydrostatic atmosphere described by primitive equations. Moisture enters in the computation of geopotential on the terrain-following levels where virtual temperature is used.

We did not spend extra space on such details as it has been discussed in previous papers where we discussed the normal-mode function projection methodology. For example, Žagar et al. (2015, Geo. Model Dev.) showed typical vertical profiles of globally averaged temperature and stability which are input to the vertical structure equation. Normal-mode functions are derived for the bounded atmosphere with lid located at the model top half-level (pressure=0, sigma = 0). The same condition is applied in NWP models and indeed in the model of ECMWF that produced the analyzed data.

With the global surface temperature specified, the equivalent depth of the first vertical mode (barotropic mode) is always about 10 km as the barotropic equivalent depth depends only on the surface temperature and the atmosphere depth (Cohn and Dee, QJRMS, 1989). Analysis of Staniforth et al. (1985) showed that the equivalent depths for subsequent internal modes are relatively insensitive to the value of the surface boundary condition, but they are sensitive to the top boundary conditions (stability and the depth of the top model layers). This means that the vertical model depth matters for the shape of the vertical structure functions. This is the reason why we analyzed only their sum i.e. the total Kelvin wave signal and not individual vertical modes.

SPECIFIC COMMENTS:

Line 5. Why do you call it a "barotropic" KW response? Shouldn't this be the baroclinic mode with a half-sinusoid vertical structure in the troposphere?

Response: Thank you for noticing this typo. The abstract has been rewritten.

Line 64. Missing "the" before "information".

Response: Corrected. Thank.

Lines 74 or 75. Change to "covers approximately 6.5 years from January 2007 until June 2013".

Response: Changed as suggested.

Line 93. "denotedm"?

Response: This typo has been corrected.

Lines 104-105. It is confusing to me to denote the KW as the $n=0$ EIG mode, since in many other papers (e.g. Matsuno 1966 and Wheeler and Kiladis 1999) the $n=0$ mode is the continuation of the mixed Rossby-gravity mode through the wavenumber 0 axis. In these papers the KW is the $n=-1$ solution.

Response: We follow derivation and classification of wave solutions of the linearized shallow-water equations on the sphere from Žagar et al. (2015, Geo. Mod. Dev.) and references therein. Enclosed is figure 1 from the paper which shows dispersion curves for four equivalent depths.

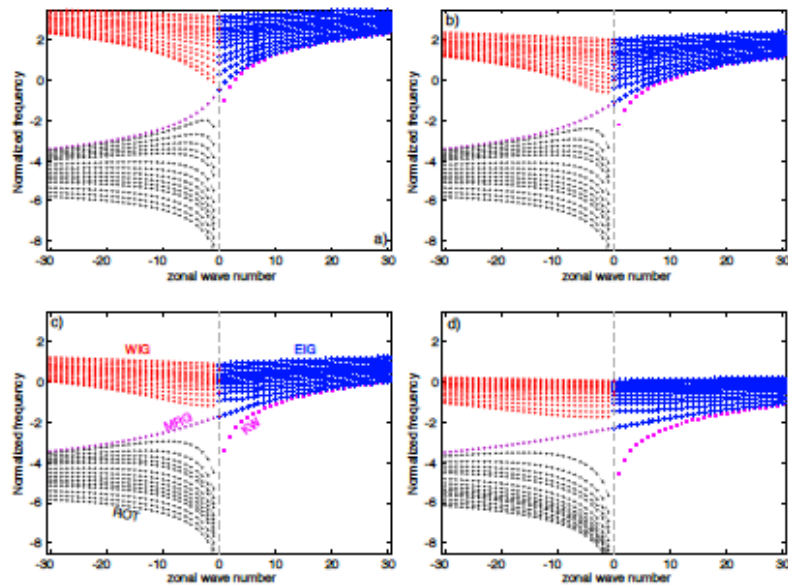


Figure 1. Frequencies of spherical normal modes for different equivalent depths. (a) $D = 10$ km, (b) $D = 1$ km, (c) $D = 100$ m and (d) $D = 10$ m. Frequencies are normalized by 2Ω factor and shown in a logarithmic scale. Frequencies of the easterly and westerly inertia-gravity modes (EIG and WIG, respectively) are shown for the meridional modes $n = 0, 1, 3, 6, 9, 14, 19, 24, 29, 34, 39, 49, 59$ and 69 . For the balanced modes (ROT), meridional modes are shown for $n = 0, 1, 3, 5, 7, 9, 14, 19, 24, 29, 34, 39, 49, 59$ and 69 . Frequencies of the Kelvin modes ($n = 0$ EIG) and MRG modes ($n = 0$ ROT) are shown by magenta-coloured symbols. Frequencies of ROT modes $n > 1$ are denoted by grey circles and interconnected by dashed black lines. The EIG and WIG mode frequencies are shown by blue and red symbols, respectively. Negative frequencies correspond to negative values of zonal wave numbers. Frequencies for $k = 0$ are zero for all ROT modes, for the MRG mode, for the Kelvin mode and for the $n = 0$ WIG mode. For $n > 0$ and $k = 0$, frequencies of the WIG modes have opposite signs and equal values as the EIG mode frequencies. For $k > 1$, frequencies of the WIG modes have larger absolute values than frequencies of the EIG modes for the same n .

Lines 138-139. I found this difficult to read because of the use of parentheses to provide the opposite meaning – please read the paper <https://eos.org/opinions/parentheses-are-not-for-references-and-clarification-saving-space>

Response: It has been changed throughout the text.

Line 141. "zonal wind" not "zonal wave".

Response: Changed as suggested.

Line 146 and many other locations. Add "the" before "Eastern hemisphere".

Response: Corrected.

Figure 4. I didn't find this figure to be very informative. A wavenumber-frequency spectrum of the Kelvin wave dataset at a few different vertical levels would have been more interesting.

Response: In the spectral i.e. modal space we can not provide the Kelvin wave energy spectrum on individual levels as we perform vertical decomposition. At each level, our KW wind and temperature perturbations include contributions from 60 spherical shallow water models meaning 60 phase speeds. While it is different from previous studies of Kelvin wave spectrum, our spectrum quantifies the vertically integrated Kelvin wave total (potential + kinetic) energy in global data. This integrated energy depends on the vertical model depth. This is a property of the global normal-mode decomposition which may be

most different from widely used single shallow-water equation system on the equatorial beta plane.

Line 221 and many other locations. What is "summer" at the equator? It doesn't make sense to call the seasons using "summer", "autumn", "winter", and "spring" for equatorial waves. I would prefer you just call them "DJF", "MAM", "JJA", "SON".

Response: Changed everywhere as suggested.

Line 260. You say "when the ENSO index is positive". Do you mean "during El Nino"?

Response: Yes. Changed as suggested.

Lines 262-265. It is perhaps also important to note that the MJO was quite strong in 2007-08 (e.g. as defined by the Real-time Multivariate MJO index), and that the MJO has been found to be generally stronger in easterly QBO years (Sun et al. 2017). I am also fairly certain that the MJO must project quite stronger onto your Kelvin wave mode.

Response: Thank you. We have updated text to include your comment on the strong MJO in this period of the strong KW activity.

Line 298. I think you mean "warm anomalies", not "heating"

Response: Changed as suggested.

Line 305. Why do you call these intramonthly KWs the "free propagating" waves? If "free" means away from the forcing of convection, then isn't every wave in the stratosphere "free"?

Response: We agree with the referee that the term "free propagating" KWs refers to the part of the Kelvin wave signal away from convective forcing, whereas in our case we discuss intramonthly KWs which are possibly coupled to convection. The revised paper uses the term "intramonthly KWs" to describe waves with periods 3-20 days.

Line 385. Please call this section "Intramonthly propagating Kelvin waves".

Response: Changed as suggested.

Figure 13. I found this very difficult to understand. On line 415 you say "different years", but what different years"? Is this a composite of all years? On line 416 you say "specific longitude". What specific longitude? The caption says it is a "climatology", but why is it so noisy if it is a climatology?

Response: The word climatology was not appropriate here. This figure is a composite of intramonthly Kelvin waves in all years as recognized by the reviewer. We have rewritten the caption and figure description in the text.

Figure 1 caption. Remove text "(panel b in Fig. 1)"

Response: Corrected

Figure 5. There appears to be some data missing at the end of 2009.

Response: The limits of x-axes in the figure were corrected. Thank you for noticing it.

Multivariate analysis of Kelvin wave seasonal variability in ECMWF L91 analyses

Marten Blaauw ¹ and Nedjeljka Žagar ¹

¹University of Ljubljana, Faculty of mathematics and physics, Ljubljana, Slovenia

Correspondence to: Marten Blaauw (marten.blaauw@fmf.uni-lj.si)

1 **Abstract.** ~~The paper presents the seasonal variability of~~

2 ~~The paper performs multivariate analysis of the linear~~ Kelvin waves (KWs) ~~represented by the operational 91-level ECMWF~~
3 ~~analyses in 2007-2013 ECMWF analyses on 91 model levels. The waves are filtered using the normal-mode function decomposition~~
4 ~~which simultaneously analyses wind and mass field based on their relationships from linear wave theory. Both spectral as well~~
5 ~~as spatiotemporal features of the KWs are examined in terms of their seasonal variability in comparison with background wind~~
6 ~~and stability. Furthermore, a differentiation is made using spectral bandpass filtering between the slow horizontal barotropic~~
7 ~~KW response and the fast vertical projection response observed as vertically-propagating KWs~~ 2007-2013 period, with focus
8 ~~on seasonal variability. The applied method simultaneously filters Kelvin wave wind and temperature perturbations in the~~
9 ~~continuously stratified atmosphere on the sphere. The spatial filtering of the three-dimensional Kelvin wave structure in the~~
10 ~~upper troposphere and lower stratosphere is based on the Hough harmonics using several tens of linearized shallow-water~~
11 ~~equation systems on the sphere with equivalent depths ranging from 10 km to a few meters.~~

12 Results ~~show~~ provide the global Kelvin wave energy spectrum. It shows a clear seasonal cycle in KW activity which is
13 ~~predominantly at the largest zonal scales (wavenumber 1-2) with the Kelvin wave activity predominantly in zonal wavenumbers~~
14 ~~1 – 2~~ where up to 50% more energy is observed during the solstice seasons in comparison with boreal spring and autumn. ~~The~~
15 ~~spatiotemporal structure of the KW reveals the slow response as a robust "Gill-type" structure~~

16 ~~Seasonal variability of Kelvin waves in the upper troposphere and lower stratosphere is examined in relation to the background~~
17 ~~wind and stability. A spectral bandpass filtering is used to decompose variability into three period ranges: seasonal, intraseasonal~~
18 ~~and intramonthly variability component. Results reveal a slow seasonal KW component with a robust dipole structure in the~~
19 ~~upper troposphere~~ with its position determined by the location of the dominant convective outflow winds throughout the
20 seasons. Its ~~maximum~~ maximal strength occurs during northern boreal summer when easterlies in the Eastern Hemisphere
21 ~~hemisphere~~ are strongest. ~~The fast response in the form of free traveling KWs occur~~ Other two components represent vertically
22 ~~propagating Kelvin waves and are observed~~ throughout the year with seasonal variability mostly found in the wave amplitudes
23 being dependent on ~~the seasonality of the~~ background easterly winds and static stability.

24 1 Introduction

25 Atmospheric equatorial Kelvin waves (hereafter KWs), first discovered in the stratosphere (Wallace and Kousky, 1968), are
26 nowadays observed and studied over a broad range of spatial and temporal scales. A broad wavenumber-frequency spectrum
27 can be traced to the spatiotemporal nature of tropical convection which generates KWs along with a spectrum of other equa-
28 torial waves. Atmospheric wave response to the stochastic nature of convection was studied by Garcia and Salby (1987) and
29 Salby and Garcia (1987) who made a distinction between (i) projection or vertical response to short-term heating fluctuations
30 (e.g. daily convection) and (ii) barotropic or horizontal response to seasonal convective heating. For KWs, the vertical response
31 gives rise to a broad frequency spectrum of vertically propagating KWs that radiate outward into the stratosphere where they
32 drive zonal-mean quasi-periodic flows such as the quasi-biennial oscillation (QBO, Holton and Lindzen, 1972). The horizontal
33 response to seasonal transitions in convective heating gives rise to planetary-scale disturbances with a half-sinusoidal vertical
34 structure confined to the troposphere. A part of this response remains stationary over the convective hotspot; its shape resem-
35 bling a classic "Gill-type" KW solution (Gill, 1980). The other part of the response intensifies and advances over the Pacific,
36 representing a transient component of the Walker circulation (Salby and Garcia, 1987).

37 Both components of the KW response received increased attention in the scientific community over the last decades in terms
38 of the role they play in the (intra)seasonal variability of the Tropical Tropopause Layer (hereafter TTL), defined as a transition
39 layer between the typical level of convective outflow at ~ 12 km where the Brunt-Väisälä frequency is at its minimum, and the
40 cold point tropopause at $\sim 16-17$ km (Highwood and Hoskins, 1998; Fueglistaler et al., 2009)(Highwood and Hoskins, 1998; Fueglistaler e
41 Within the TTL, temperature variations play an important role in controlling the stratosphere-troposphere exchange of vari-
42 ous species such as ozone and water vapour thereby aiding in the dehydration process of air entering the stratosphere. The
43 two parts of the KW response ~~alternate-modulate~~ the TTL differently on different time scales (Highwood and Hoskins, 1998;
44 Randel and Wu, 2005; Ryu et al., 2008; Flannaghan and Fueglistaler, 2013); their relative contribution to TTL dynamics varies
45 with season and is not yet fully understood. The present study contributes to this topic by applying a novel multivariate analysis
46 of Kelvin wave seasonal variability in model-level analysis data.

47 Seasonal variations of Kelvin wave dynamics in the TTL have been previously studied using temperature data derived
48 from satellites such as SABER (Sounding of the Atmosphere using Broadband Emission Radiometry, Garcia et al., 2005;
49 Ern et al., 2008; Ern and Preusse, 2009), HIRDLS (High Resolution Dynamics Limb Sounder, Alexander and Ortland, 2010),
50 and GPS-RO (Global Positioning System Radio Occultation, Tsai et al., 2004; Randel and Wu, 2005; Ratnam et al., 2006).
51 For example, Alexander and Ortland (2010) reported a clear seasonal cycle around 16-17 km (~ 100 hPa) in KW temperature
52 observed by HIRDLS, coinciding closely with variations in background stability. A widely used method for the KW filtering
53 from gridded data is the space-time spectral analysis introduced by Hayashi (1982). ~~It-Space-time spectral filtering assumes~~
54 ~~that the linear adiabatic theory for equatorial waves on a resting atmosphere is applicable (Gill, 1982). Filtering~~ operates on
55 single variable data and it has been widely used to diagnose equatorial waves in the outgoing longwave radiation (OLR, e.g.
56 Wheeler and Kiladis, 1999) and climate model outputs (e.g. Lin and Coauthors, 2006). Based on 40-year ECMWF reanalysis
57 (ERA-40) data, Suzuki and Shiotani (2008) found that the temperature component of Kelvin waves tends to peak at 70 hPa

58 while the zonal wind peaks at lower altitudes, i.e. at 100 hPa (and 150 hPa) in Eastern (Western) hemisphere in Eastern and
59 Western hemisphere, respectively.

60 The zonal wind and geopotential height of the KW are closely related. For a single zonal wavenumber k , the geopotential,
61 Φ_{kw} , and the zonal wind U_{kw} of a zonally propagating KW are related according to the following equation: On the equatorial
62 β -plane, shallow-water linear wave theory describes the Kelvin wave geopotential height (h_{kw}) and zonal wind (u_{kw}) perturbations
63 propagating zonally with phase speed c as (Matsumo, 1966):

$$64 \quad \Phi_{kw} = g h_{kw}(x, y) = \frac{\nu c}{k g} U_{kw}, \quad \text{where} \quad U_{kw}(x, y) = U_0 \exp\left(-\frac{\beta k y^2}{2\nu} - \frac{\beta y^2}{2c}\right) \cos k(x - ct). \quad (1)$$

65 Here, U_0 is the KW amplitude in zonal wind on u_0 is the zonal wind amplitude at the equator, $\beta = 2\Omega/a$ (Ω being the
66 rotation rate and a the radius of Earth), ν is the wave frequency, g is gravity and y is the distance from the equator.
67 These expressions are obtained as a special solution of the linearized shallow-water equations on the equatorial β -plane
68 (e.g. Holton, 2004, Chapter 11). The $\beta = df/dy$, f being the Coriolis parameter. The dispersion relationship between the
69 wave frequency ν and the zonal wavenumber k is $\nu = kc$. The gravity wave speed in a layer of homogeneous fluid with mean
70 depth D is given by $c = \sqrt{gD}$ (Gill, 1982).

71 The KW e -folding decay width, a_e , known as the equatorial radius of deformation, is given by $a_e = (c/2\beta)^{1/2}$, where
72 the KW phase speed c is determined from the dispersion relation $\nu = kc$. By prescribing the value of KW phase speed c (i.e.
73 the equivalent depth of the shallow-water equation system), analytical solutions from linear wave theory D , the horizontal
74 structure of KW is defined by (1) for any k and can be used to simultaneously analyze wind and height data of the KW wave
75 geopotential height perturbations due to KW waves on a single horizontal level. Such multivariate analysis was carried out
76 by Tindall et al. (2006) who analyzed several levels the ECMWF 15-year reanalysis dataset (for the lower stratosphere for
77 the ERA-15) in the lower stratosphere. They reported a maximum of Kelvin wave activity at 100 hPa around the solstices
78 when tropical cloud activity maximizes. For the ERA-15 data in 1981-93 period, their Kelvin wave analysis explained. Their
79 results suggested that KWs contributes approximately 1 K² of the temperature variance on the equator with peak activity
80 occurring during solstice seasons at 100 hPa, during December-February at 70 hPa and at 50 hPa it occurs during the
81 easterly to westerly quasi-biennial oscillation (QBO) phase transition. Yang et al. (2003) used a_e as the fitting parameter for
82 the projection of the ERA-15 data on the meridional structure of the KW and other equatorial waves. They found that the best
83 fit trapping scale within 20°N-20°S is around 6°. The multivariate projection of data on the horizontal structures of equatorial
84 waves including KWs on the equatorial β -plane was performed also for the short-range forecast errors of the ECWMF model
85 (Žagar et al., 2005, 2007). For example, Žagar et al. (2007) found that forecast errors within 20°N-20°S belt project on KWs
86 significantly more in the easterly QBO phase than in the westerly phase.

87 The present paper extends the use of linear wave theory from In this paper we extend the linear Kelvin wave analysis based
88 on the shallow-water equation theory on the equatorial β -plane to the sphere. Second, we extend the KW filtering on individual
89 horizontal levels or vertical planes to the three-dimensional (3D) spherical coordinates in order to analyze KW analysis
90 simultaneously in wind and temperature fields in recent ECMWF operational analyses. We focus on. This study thus explores
91 seasonal variability of KWs in the TTL layer in the ECMWF operational analyses during a period when the model employed

92 91-vertical level (L91) between the surface and 1 Pa. The L91 model was in operations between 2006 and early summer 2013
93 when it was replaced by 137 levels. This study thus explores most of a multivariate fashion using most of the information
94 on the vertical structure of KWs available in the L91 analysis data. We present a methodology for the simultaneous analysis
95 of wind and temperature perturbations associated with KWs with respect to the background state and apply it to quantify
96 scale-dependent seasonal KW variability in several frequency bands. wave structure available in recent operational ECMWF
97 analyses.

98 The paper consists of five sections. Methodology On the sphere, the Kelvin mode is the slowest eastward-propagating
99 eigensolution of the shallow-water equations (or Laplace tidal equations) linearized around a state of rest (e.g. Kasahara, 1976).
100 In the continuously stratified atmosphere, the depth D becomes the "equivalent depth" of a given baroclinic mode and we need
101 to solve Laplace tidal equations for a range of D from large (corresponding to the barotropic structure) to rather small (for
102 high baroclinic modes) in order to consider the spectrum of Kelvin waves (e.g. Boyd, 2018). In contrast to the Kelvin wave
103 trapping on the equatorial β -plane, which is controlled by a_e i.e. by the equivalent depth, the degree of the KW diagnosis
104 and the data are presented in section 2 equatorial confinement on the sphere is in addition controlled by the zonal wavenumber
105 (Boyd and Zhou, 2008). As shown by Boyd and Zhou (2008), even barotropic KW with D around 10 km are on the sphere
106 confined within the tropical belt.

107 In section 2 we present a methodology which diagnosis 3D Kelvin waves in spherical datasets. Section 3 presents the
108 KW energetics in wavenumber space focusing on the seasonal cycle. Section 4 presents a 3D view on KWs in L91 dataset,
109 seasonal KW variability in several frequency bands both for the horizontal as well as for the vertical projection KW response.
110 Conclusions and outlook are given in section 5.

111 2 Data and methodology

112 The Kelvin waves are filtered using the Normal-Mode-Function-normal-mode function (NMF) decomposition derived by
113 Kasahara and Puri (1981) and briefly summarized below, formulated as the *MODES* software package by Žagar et al. (2015).
114 Here the methodology is briefly summarized followed by the method for the computation of the KW temperature perturbations
115 and by examples of the 3D KW structure in global data.

116 Input ECMWF operational analyses cover 6 covers approximately 6.5 years from January 2007 till June 2013, approximately
117 6.5 years, untill June 2013. The dataset starts after two important updates in the ECMWF assimilation cycle: a resolution update
118 on 1 February 2006 and the introduction of GPS-RO temperature profiles in the assimilation on 12 December 2006. The data
119 ends at the next update in vertical resolution from L91 to L137 on 25 June 2013. The data horizontal resolution is 256×128
120 points in the zonal and meridional directions (regular Gaussian grid N64), respectively, on 91 irregularly spaced hybrid model
121 levels up to around 0.01 hPa (around 80 km). The temporal resolution is 6 hours, i.e. 4 times per day, at 00, 06, 12 and 18 UTC.
122 A case study of the large-scale KW in July 2007 (Žagar et al., 2009) showed how in this dataset by Žagar et al. (2009) showed
123 that the NMF method provides information on the horizontal and vertical 3D wave structure and its vertical propagation in the

124 stratosphere. [Another case study from the same month demonstrated how the vertical KW structure improves as the number of](#)
 125 [vertical levels increased \(Žagar et al., 2012\).](#)

126 2.1 Filtering of Kelvin waves by 3D normal-mode function expansion

127 The basic assumption behind the NMF expansion is that a global state of the atmosphere described by its mass and wind vari-
 128 ables at any time can be considered as a superposition of the linear wave solutions upon a predefined background state. ~~These~~
 129 ~~linear solutions describe two types of wave motions: Rossby waves and inertio-gravity waves which obey their corresponding~~
 130 ~~dispersion relationships. The associated eigensolutions in terms of the Hough harmonics define both mass and wind fields of~~
 131 ~~the waves. The linear wave theory approach has been successfully employed in many studies, especially for the large-scale~~
 132 ~~tropical circulation features (e.g. Gill, 1980; Salby and Garcia, 1987; Garcia and Salby, 1987).~~

133 The NMF decomposition derived by Kasahara and Puri (1981) uses the σ ~~coordinates and a vertical coordinate and linearization~~
 134 ~~around the state of rest and~~ realistic vertical temperature and stability stratification. 3D wave solutions of ~~primitive equations~~
 135 ~~linearized around the state of rest~~ [linearized primitive equations](#) are represented as a truncated time ~~serie series~~
 136 harmonic oscillations and the vertical structure functions. The [assumption of separability leads to separate equations for the](#)
 137 [vertical structure and horizontal oscillations. The latter are known as shallow-water equations on the sphere or Laplace tidal](#)
 138 [equations without forcing. The two systems are coupled by a separation parameter \$D\$ which is called the equivalent height](#)
 139 [\(Boyd, 2018\). Eigenmodes of the global shallow-water equations are known as Hough harmonics. They describe two types of](#)
 140 [wave motions: Rossby waves and inertio-gravity waves which obey their corresponding dispersion relationships on the sphere.](#)

141
 142 [The expansion of a global input data vector \$\mathbf{X}\(\lambda, \varphi, \sigma\) = \(u, v, h\)^T\$ can be represented by a discrete finite series as:](#)

$$143 \begin{pmatrix} u(\lambda, \varphi, \sigma) \\ v(\lambda, \varphi, \sigma) \\ h(\lambda, \varphi, \sigma) \end{pmatrix} = \sum_{m=1}^M \mathbf{S}_m \left[\sum_{n=1}^R \sum_{k=-K}^K \chi_n^k(m) \mathbf{H}_n^k(\lambda, \varphi; m) \right] G_m(\sigma) \quad (2)$$

144 The [input data vector contains wind components \$u, v\$ and the transformed geopotential height \$h\$ defined as \$h = g^{-1}P\$ where](#)
 145 [\$g\$ is the gravity and \$P\$ is defined as: \$P = \Phi + RT_0 \ln\(p_s\)\$; that is, it is the sum of geopotential \$\Phi\$ and a surface pressure, \$p_s\$, term.](#)
 146 [Other two variables represent the specific gas constant for dry air \(\$R\$ \) and the globally-averaged vertical temperature profile](#)
 147 [\(\$T_0\(\sigma\)\$ \). The zonal and vertical truncations \(\$K\$ and \$M\$, respectively\) define ~~maximum maximal~~ numbers of zonal waves at a
 148 single latitude \(wavenumber \$k\$ \) and a maximal number of vertical modes ~~denoted \$m\$ respectively.~~ \(denoted \$m\$ \) respectively. For
 149 \[every vertical structure eigenfunctions \\$G_m\\(\sigma\\)\\$, Hough harmonic functions, \\$\mathbf{H}_n^k\\(\lambda, \varphi\\)\\$ describe non-dimensional oscillations in\]\(#\)
 150 \[the horizontal plane of the fluid with the mean depth equal the equivalent depth \\$D_m\\$. The parameter \\$D_m\\$ appears in Eq. \\(2\\) in\]\(#\)
 151 \[the diagonal matrix \\$\mathbf{S}_m\\$ with elements \\$\\(gD_m\\)^{1/2}\\$, \\$\\(gD_m\\)^{1/2}\\$ and \\$D_m\\$ which normalizes the input data vector after the vertical\]\(#\)
 152 \[projection and thereby removes dimensions.\]\(#\) Parameter \$R\$ is the total number of meridional modes which is a sum of the
 153 eastward inertio-gravity waves \(EIG\), westward inertio-gravity waves \(WIG\) and Rossby waves. ~~Oscillations in the horizontal~~
 154 ~~plane are given in terms of Hough harmonic functions, \$\mathbf{H}_n^k\(\lambda, \varphi\)\$ for every vertical structure eigenfunctions \$G_m\(\sigma\)\$. The~~](#)

155 horizontal and vertical solutions are connected by the equivalent depth parameter D_m , which appears in Eq. (2) in the diagonal
 156 matrix \mathbf{S}_m with elements $(gD_m)^{1/2}$, $(gD_m)^{1/2}$ and D_m . Linearization about the state of rest is not a drawback of the method as
 157 wave frequencies are used solely for the formulation of the projection basis and not for studying wave propagation properties.
 158 As shown by Kasahara (1980) (see also its Corrigendum) the meridional structures of the Hough functions for large scales are
 159 not significantly different if the linearization is performed around the non-zero mean zonal flow. The impact of latitudinal shear
 160 on the Kelvin waves was shown negligible by Boyd (1978). Further details of the applied NMF representation NMF projection
 161 procedure are given in Žagar et al. (2015).

162 The input data vector contains wind components u, v and the geopotential height h defined as $h = g^{-1}P$ where g is the
 163 gravity and P is a modified geopotential given by: $P = \Phi + RT_0 \ln(p_s)$, i. e. the sum of the geopotential field Φ and a
 164 surface pressure p_s term. Other two variables represent the specific gas constant for dry air (R) and the globally-averaged
 165 vertical temperature profile (T_0). The For each zonal wavenumber, the Kelvin mode is the lowest eastward-propagating
 166 latitudinal Hough function. In (2), the Kelvin wave is represented by the nondimensional complex expansion coefficients
 167 $\chi_n^k(m)$ represent both geopotential height and wind perturbations due to waves. The Kelvin mode is represented in (2) by
 168 the first eastward-propagating IG mode. Although our meridional index starts from 1 (to follow otherwise used notation) with
 169 the meridional index $n = 1$. However, to follow often used notation, we shall denote KW in the remainder the Kelvin wave
 170 in the remainder of this study as the $n = 0$ EIG mode, i.e. the KWs are given Kelvin wave wind and geopotential height are
 171 represented by coefficients $\chi_{kw} = \chi_0^k(m)$.

172 In our application to the L91 ECMWF dataset, we used data on the N64 Gaussian grid and 91 model levels with model
 173 top located at 0.01 hPa (around 80 km). Data are analyzed 4 times per day, at 00, 06, 12 and 18 UTC. The pre-processing
 174 step consists of the interpolation of winds and geopotential from the hybrid ($\sigma-p$) levels to σ levels after geopotential Φ
 175 is computed on the hybrid levels. The The truncation values are $K = 55$ $K = 85$ and $M = 60$. This means that KW signal
 176 in 3D circulation at a single time instant consists of 5100 waves, 85 waves in every shallow-water equation system. Higher
 177 vertical modes were left out as their contribution equivalent depth is smaller than 2 meters and their contribution to the total
 178 KW signal is negligible in the outputs in the TTL and the stratosphere. The relation between the truncation parameters and the
 179 normal-mode projection quality is discussed in Žagar et al. (2015) and references therein.

180 Once the forward projection is carried out and coefficients $\chi_n^k(m)$ are produced, filtering of KWs in physical space can be
 181 performed through (2) after setting all χ , except those representing the KWs, to zero. The result of filtering are fields u_{kw} ,
 182 v_{kw} and h_{kw} which provide the KW zonal wind, meridional wind and geopotential height perturbations. Notice here that in
 183 contrast to the equatorial β -plane, KWs on the sphere have a very small meridional wind component which is thus left out
 184 from the discussion (Boyd, 2018).

185 The KW temperature perturbation, T_{kw} can be derived from the h_{kw} fields on σ levels using the hydrostatic relation in σ
 186 coordinates:

$$187 \quad T_{kw} = -\frac{g\sigma}{R} \frac{\partial h_{kw}}{\partial \sigma}. \quad (3)$$

188 The orthogonality of the normal-mode basis functions provides KW energy as a function of the zonal wavenumber and
 189 vertical mode. After the forward projection, the energy spectrum of total (potential and kinetic) energy for each Kelvin wave
 190 can be computed using the energy product for the k th and m th normal modes (Žagar et al., 2015) as:

$$191 \quad I_{\text{kw}}(k, m) = \frac{1}{2} g D_m \chi_{kw} [\chi_{kw}]^* . \quad (4)$$

192 The units are J kg^{-1} . The KW global energy spectrum as a function of the zonal wavenumber is obtained by summing energy
 193 in all vertical modes:

$$194 \quad I_{\text{kw}}(k) = \frac{1}{2} \sum_{m=1}^M g D_m \chi_{kw} [\chi_{kw}]^* . \quad (5)$$

195 2.2 Examples of 3D structure of Kelvin waves in L91 analyses

196 Kelvin waves are shown in Fig. 1-2 for a few days in July 2010 to introduce and illustrate their properties as filtered by the
 197 NMF methodology. ~~The second part of July 2010 was characterized by an abundance in both vertically propagating as well as~~
 198 ~~quasi-stationary KW structures throughout the atmosphere.~~

199 Figure 1 illustrates the meridional structure of Kelvin waves on 25 July 2010 on 2 levels. KW activity was found largest in
 200 the zonal wind component at 150 hPa over the Indian Ocean. The geopotential dipole structure is ~~centered-centred~~ over the
 201 convective hotspot over the Maritime continent. At 100 hPa, we find largest amplitude of KW temperature perturbations up to
 202 4 K positioned above the zonal wind maxima at 150 hPa. The meridional wind component of the KW is nonzero in spherical
 203 coordinates, but is at most 0.22 ms^{-1} at 100 hPa which is negligible compared to the zonal wind component (maximum 12.5
 204 ms^{-1}) making the KW wind field primarily zonal. Note that the presented horizontal structure at a single level is a superposition
 205 of 60 vertical modes, i.e. 60 shallow water models with equivalent ~~depts-depths~~ from about 10 km to a couple of meters.

206 Figure 2 ~~can be discussed in relation to Eq. . It states that the amplitude of the cold (warm) KW temperature perturbation~~
 207 ~~is proportional to the negative (positive) vertical gradient in geopotential, as well as in zonal wind since zonal wind and~~
 208 ~~geopotential components are in phase. Horizontally, the cold anomaly is always located between the westerly and the easterly~~
 209 ~~phase of the zonal wave component. Vertically, maximum positive temperatures are observed between easterly winds below and~~
 210 ~~westerly winds above. A rough estimation can be made of the vertical wavelength based on alternating zonal wind minima and~~
 211 ~~maxima. For example, on 31 July a quasi-stationary vertical wave structure with extension in the stratosphere located around~~
 212 ~~60°E has easterly winds located at 50 hPa illustrates day-to-day filtered KW fields along the equator on three separate July days~~
 213 in 2010, namely 25, 28 and 31. Both zonal wind (~ 21.5 km) and 150 hPa (~ 13.5 km), which makes a vertical wavelength
 214 of around 8 km. blue-to-red shades) and temperature fields (red contours) are shown. Without any predefined constrains on the
 215 KW propagation, one can observe a rich variety of KW behaviour occurring in time: from the quasi-stationary dipole patterns
 216 centred at 160 hPa to a wave package of free propagating wave structures in the stratosphere transiting from the western into
 217 the eastern hemisphere.

218 In the stratosphere, ~~above 80 hPa, strong KW activity was present in the form of free waves propagating the uppermost~~
 219 easterly wind component in blue shades around 30 – 50 hPa moves in eastward and downward ~~, therefore with direction,~~

220 demonstrating the upward transport of KW energy (Andrews et al., 1987). KW amplitudes were largest over Eastern hemi-
221 sphere with temperatures up to 4 K and zonal winds up to 12 ms^{-1} . The large amount of KW activity occurred during the
222 easterly phase of the QBO with strong easterly winds present between 30 and 80 hPa (not shown), providing favourable con-
223 ditions for ~~the waves to propagate upward~~strong KW activity.

224 Between 100 and 200 hPa during the second half of July, there was low-frequency KW activity present in the form of a
225 stationary and robust "wave-1" pattern with strong KW easterly winds up to 24 ms^{-1} in Eastern Hemisphere and KW westerly
226 winds up to 10 ms^{-1} in the Western Hemisphere. The high vertical resolution within the TTL resolves shallow KW structures
227 and a typical slanted structure towards the east in KW easterlies as well. The appearance and strength of horizontal KW
228 response coincides with the presence of strong easterly winds in the TTL in the Eastern Hemisphere during this period (not
229 shown). Figure 2 also shows that below 300 hPa the KW activity decreases and we shall not discuss levels under 300 hPa in
230 the paper.

231 The zonal wind and temperature components are coupled through Eq. (3) which states that the amplitude of the negative
232 KW temperature perturbation is proportional to the negative vertical gradient in geopotential (and vice versa), as well as in the
233 zonal wind since the zonal wind and geopotential are in phase. Horizontally, the cold anomaly is always located between the
234 westerly and the easterly phase of the zonal wind component. Vertically, maximal positive temperatures are observed between
235 easterly winds below and westerly winds above. An estimate of the vertical wavelength can be made based on alternating zonal
236 wind minima and maxima. For example, on 25th July a well-developed KW package extending into the stratosphere moved
237 from the Western into the Eastern hemisphere. A quasi-stationary component of the wave package is observed around 60°E
238 with easterly winds located at 50 hPa ($\sim 21.5 \text{ km}$) and 150 hPa ($\sim 13.5 \text{ km}$), implying a vertical wavelength of around 8 km.

239 More examples based on daily basis filtered from the 10-day deterministic forecast of the ECMWF can be found on the
240 MODES website¹.

241 2.3 Other data and impact of the background state

242 In addition to the outputs from modal decomposition, full zonal wind and temperature fields from ECMWF analyses are used
243 to compute the background fields based on the same N64 grid and over the same period (Jan 2007 - Jun 2013). Zonal wind U
244 and static stability N are latitudinally averaged in the belt 5°S - 5°N on all model levels to produce their zonal structure.

245 Static stability profiles are estimated through

$$246 \quad N^2 = \frac{g^2}{\Theta} \frac{\partial \Theta}{\partial \phi} \quad (6)$$

247 in units of s^{-2} and are defined on hybrid model levels on which the geopotential field ϕ and the potential temperature field Θ
248 are derived a priori from the input data. Both fields are shown in Fig. 3.

249 The zonal wind field has the largest values on average in the TTL around 150 hPa with westerly winds peaking in the Western
250 Hemisphere over the Pacific Ocean and easterly winds peaking in the Eastern ~~Hemisphere~~ hemisphere over the Indian Ocean
251 and Indonesia. It represents a typical time-averaged outflow pattern in response to tropical convection (e.g. Fueglistaler et al.,

¹<http://meteo.fmf.uni-lj.si/MODES/>

252 2009). Throughout the seasons there is a longitudinal shift of this pattern following the convective source which is most clearly
253 observed at 150 hPa. Such seasonal shift is visible up to 100 hPa in Fig. 3(b) where winds are weaker compared to 150 hPa.
254 In northern winter, zonal winds are strongest over Indonesia and [the](#) Eastern Pacific with the zonal wind maxima position and
255 strength similar compared to the longer ERA-40 dataset used by Suzuki and Shiotani (2008). During [northern-boreal](#) summer
256 easterly winds mainly prevail over the Indian Ocean, which is linked to the Indian Monsoon season.

257 At 100 hPa, the static stability illustrates the strongest seasonal cycle with values ranging from near-tropospheric values
258 of $3 \times 10^{-4} \text{ ms}^{-2}$ during northern winter towards stratospheric values of $5 - 6 \times 10^{-4} \text{ ms}^{-2}$ during [northern-boreal](#) summer.
259 Note also the resolved local maxima in static stability at 80 hPa above the warm pools, known as the Tropical Inversion
260 Layer (TIL) and which is possibly wave-driven (Grise et al., 2010; Kedzierski et al., 2016). Figure 3(b) suggests that the TIL
261 descends down to 100 hPa during [the-boreal](#) summer months peaking over Western Pacific, in agreement with the cycle found
262 in GPS-RO observations by Grise et al. (2010).

263 Kelvin waves are subject to wave modulation in changing background environments. Along its trajectory, the potential
264 energy of the KW changes with varying background winds and stability which can be largely described by linear wave theory
265 as long as waves are not near their critical level involving breaking and dissipation (Andrews et al., 1987). For simplification,
266 KW modulation can be examined for the case of pure zonal as well as pure vertical wave propagation based on the wave
267 modulation analysis performed by Ryu et al. (2008). A few key points on their local wave action conservation principle are
268 [summarized-summarised](#) in the following.

269 In the tropical atmosphere, zonal modulation is the dominant process for KWs propagating in the stratosphere and in all
270 non-easterly winds in the TTL. Vertical modulation becomes important in the presence of easterly winds within the TTL.
271 Zonal modulation is found to affect both u_{kw} and T_{kw} components and their amplitudes are proportional to the Doppler-
272 shifted phase speed by $(c - U)^{1/2}$ in case of pure zonal propagation direction. This means that Kelvin waves diminish in
273 amplitude over regions with westerly winds and become more prone to dissipative processes, while amplify over regions with
274 easterly winds². In case of pure vertical modulation, the change in wave potential energy mainly [resonates-fluctuates](#) with the
275 temperature component of the Kelvin wave. Along the rays' vertical path, the waves amplitude is proportional to the Brunt-
276 Väisälä frequency as $\propto N^{3/2}$, and to the Doppler-shifted phase speed as $\propto (c - U)^{-1/2}$, such that N is expected to play a
277 primary role above 120 hPa where its value starts increasing rapidly (see Fig. 3).

278 Alexander and Ortland (2010) showed through wave modulation principles that temporal variations in zonal-mean N indeed
279 are correlated with observed KW amplitudes at 16 km (approx. 100 hPa). A more extensive wave modulation analysis was
280 described by Flannaghan and Fueglistaler (2013) using the full ray tracing equations to demonstrate that zonal winds in the TTL
281 not only modulate Kelvin waves locally, but also create a lasting modulating effect on wave activity through ray convergence
282 in the stratosphere. In particular, the seasonal cycle of the upper tropospheric easterlies (on average located over the western
283 Pacific), that acts as an escape window for Kelvin waves throughout the year and largely explains the longitudinal structure of
284 Kelvin wave zonal wind and temperature climatology.

²Keeping in mind that vertical wave propagation and consequently modulation becomes increasingly important as well wherever easterly winds are strong.

285 We shall present the seasonal variability of tropical convection by using the Outgoing Longwave Radiation (OLR) dataset
286 with daily outputs from the NOAA Interpolated OLR product (Liebmann and Smith, 1996). The OLR product, often used as
287 a proxy for convection, is extracted on a $2.5^\circ \times 2.5^\circ$ grid and interpolated on a N64 grid. Latitudal-Latitudinal averages are
288 derived over larger domain, namely over 15°S - 15°N since organized convection tend to happen more remote from the equator,
289 especially during the summer monsoon season over the Asian continent.

290 3 Kelvin wave energetics

291 We start with ~~an overview of a discussion of the~~ KW energy distribution among ~~the~~ zonal wavenumbers as given by (5),
292 followed by ~~the seasonal cycle of KW energy as a function of zonal wavenumber.~~ seasonal differences.

293 3.1 Energy distribution of Kelvin wave

294 The seasonal cycle in the energy-zonal wavenumber spectra is shown in Fig. 4 after summing up over all vertical modes. On
295 average, energy decreases as the zonal wavenumber increases as typical for atmospheric energy spectra. As we deal with the
296 large scales, we show only the first six zonal wavenumbers with energy values shown separately for the annual mean and the
297 four seasons separately.

298 Figure 4 shows that largest seasonal variations in KW energy are found at the largest zonal scales. For all zonal wavenumbers,
299 above annual-mean energy values are observed during ~~winter and summer seasons while autumn and spring~~ DJF and JJA
300 seasons while SON and MAM are below annual-mean energy. In the zonal wavenumber 1, total KW energy varies between
301 200 Jkg^{-1} in MAM season and somewhat over 300 Jkg^{-1} in JJA. In wavenumber 2, values do not exceed 100 Jkg^{-1} and
302 JJA still contains the largest energy. At higher wavenumbers, DJF season becomes the most energetic. In $k > 4$, total KW
303 energy is under 20 Jkg^{-1} and continue to reduce with k . The slope of the KW energy spectrum is between $-5/3$ and -1 at
304 planetary scales (not shown), similar to the spectra presented in Žagar et al. (2009) for July 2007 data. The ~~summer-JJA~~ summer-JJA spectra
305 has on average the steepest slope compared to other seasons, in particular the ~~winter-DJF~~ winter-DJF spectra. The energy distribution on
306 planetary scales is mainly associated with large-scale tropical circulation established in response to ongoing tropical convection.
307 Therefore, the zonal distribution of tropical convection may likely play a crucial role in explaining ~~winter and summer~~ DJF
308 and JJA season differences of KW energy, which will be explored in next section.

309 3.2 Seasonal cycle of KW energy

310 Figure 5 illustrates more details on the seasonal cycle by showing KW energy time series at the largest scales represented by
311 zonal wavenumbers $k = 1$, $k = 2$ and remaining scales $k > 2$. During most ~~summers~~ JJA seasons and occasionally in ~~winter~~
312 DJF (e.g. 2008) the total amount of KW energy in $k = 1$ can reach up to 600 Jkg^{-1} , or twice the ~~summer-JJA~~ summer-JJA average.
313 The minimum in $k = 1$ KW energy mainly occurs during October ~~month~~ followed by April with values dropping towards
314 100 Jkg^{-1} , or half the ~~autumn-SON~~ autumn-SON average. The temporal pattern in $k = 2$ is similar to the $k = 1$ pattern, but with a less

315 pronounced semiannual cycle with maximum values up to 200 Jkg^{-1} and minimum values towards 30 Jkg^{-1} . On zonal scales
316 $k > 2$, KWs still show a semiannual cycle with highest vertically-integrated values of energy ~~over winter seasons~~ in DJF.

317 In particular, for zonal wavenumber $k = 1$ one can distinguish ~~inter-monthly~~ intermonthly in addition to semiannual vari-
318 ability. ~~Inter-monthly~~ Intermonthly variability is most clearly observed during ~~northern summer~~ JJA, for example in July 2011
319 where one can distinguish six separate peaks of over 400 Jkg^{-1} energy over a period of approximately 90 days resembling
320 an average wave period of about 18 days. These are typical periods for free propagating Kelvin waves as observed in the
321 TTL and lower stratosphere (e.g. Randel and Wu, 2005). Note here again that our KW energy is vertically integrated over the
322 whole model depth. This means that the observed intermonthly variability of KWs appears dominated by the cyclic process of
323 free propagating KWs entering the TTL, amplifying due to changing environmental conditions, followed by wave breaking or
324 dissipation.

325 The dominant scales of temporal variability in KWs are illustrated by a frequency spectrum of $k = 1$ in Fig. 6. The spectrum
326 is produced by ~~a the~~ Fourier transform of energy data time series of 6.5 years ~~to frequency space~~. The resulting power
327 spectrum has been smoothed by taking the Gaussian-shaped moving averages over the raw spectrum by using ~~a the~~ Daniell
328 kernel three times (Shumway and Stoffer, 2010). The spectrum ~~shows a clear~~ contains a peak at 1-day period ~~representing~~
329 ~~tidal variability in KWs~~ associated with the diurnal tide partially projecting on the Kelvin waves. After that, a gradual increase
330 of energy is seen towards the 16-day period with multiple individual periods standing out. For periods longer than 20 days,
331 individual peaks are found close to 25, 43 and 59 days. After that, most KW energy is contained by far in the semiannual cycle.
332 The frequency spectrum provides ~~an a~~ useful starting point for the discussion in the next section when the spatiotemporal
333 patterns of KWs shall be examined in several spectral domains.

334 Returning to Fig. 5, a low-pass filter with 90 day cut-off has been applied on KW energy in order to keep only the two
335 main spectral peaks in Fig. 6. The result is visible as the thicker black line in Fig.5 for all three zonal wavenumber groups. A
336 semiannual cycle for all zonal wavenumbers is evident with most energy observed around January and July, while least energy
337 is observed approximately one month after the equinoxes. During the years 2007, 2010, 2011, and 2012, more $k = 1$ KW
338 energy is observed during ~~summer~~ JJA compared to the follow-up ~~winter~~. ~~The winter~~ DJF season. ~~The DJF~~ of 2009-2010 was
339 for example above average with energy values for $k = 1$ above 350 Jkg^{-1} .

340 The year to year differences can be explained by many coupled factors: ~~-,~~ In general, one expects ~~the~~ vertically-integrated
341 KW activity to increase when background wind conditions become favorable, i.e. in the presence of easterly winds. This
342 occurs in the TTL in relation to strong convective outflow (Garcia and Salby, 1987; Suzuki and Shiotani, 2008; Ryu et al.,
343 2008; Flannaghan and Fueglistaler, 2013) during ~~winter and summer~~ DJF and JJA seasons mainly. Moreover, ~~one can expect~~
344 ~~enhanced KW activity whenever the easterly QBO cycle is present in the~~ KW activity is enhanced whenever easterly QBO
345 winds are present down into the lower stratosphere (Baldwin and Coauthors, 2001; Alexander and Ortland, 2010) or ~~when the~~
346 ~~ENSO index is positive during El Niño~~ (Yang and Hoskins, 2013). The latter factor ~~might explain partly the~~ may partly explain
347 a large difference in the ~~abundant amount of~~ KW energy during the El Niño ~~winter~~ DJF of 2009-2010 and the below-average
348 ~~amount of KW energy~~ energy level a year after, during the strong La Niña ~~winter~~ DJF period of 2010-2011. However, during
349 the La Niña ~~winter~~ DJF of 2007-2008, the amount of KW energy is ~~observed to be~~ above normal. That ~~winter~~ season was

350 however characterized by ~~favorable~~ above-normal MJO activity which often occurs during favourable easterly QBO conditions
351 in the stratosphere ~~while during the winter of~~ (Son et al., 2017). During 2010-2011 DJF season stratospheric winds were largely
352 westerly ~~of nature~~ thereby prohibiting KW activity. The role of these low-frequency atmospheric phenomena on KW seasonal
353 variability is a topic of further research.

354 Finally, Fig. 5 also shows that KW activity in July 2007, previously examined by Žagar et al. (2009), was ~~an exceptionally~~
355 ~~energetic month~~ exceptionally strong. A large part of that energy, ~~approximately 400 Jkg⁻¹ (52.7% of total KW energy), was~~
356 ~~projected on~~ (somewhat more than half) belonged to zonal wavenumber 1. In spatiotemporal terms, it ~~represented~~ is associated
357 with the presence of a strong dipole structure in the TTL (as in Fig.2), which is colocated with favourable easterly wind
358 conditions in the TTL as well as in the stratosphere (not shown). In fact, at 50 hPa the QBO was just at the beginning of its
359 easterly phase in July 2007.

360 4 A spatiotemporal view on Kelvin wave seasonal variability

361 4.1 Kelvin wave decomposition among wave periods

362 In this section, the spatiotemporal view of KWs shall be presented over three dominant ranges of wave periods in Fig. 6,
363 namely: (i) the (semi)annual cycle using a low-pass filter with cut-off period at 90 days, (ii) the intraseasonal period using
364 a bandpass filter over periods between 20-90 days, and finally (iii) the intramonthly period with bandpass filtered periods
365 between 3-20 days. The ~~choice of ranges~~ chosen periods, especially the intramonthly periods ~~is related to previous studies using~~
366 ~~observations. For all three cases, mean 6-year,~~ are similar to those used in previous studies. In each case, mean 6-year fields as
367 well as seasonal means shall be presented.

368 Note that our temporal filtering operates on time series of KW signals at every grid point. This is different from the
369 commonly applied space-time filtering following Hayashi (1982) that applies KW dispersion relations. Our filtered KWs can
370 appear stationary or even westward shifted due to westward-moving sources of the KW amplification (e.g. easterly winds, high
371 static stability in the TTL).

372 Both KW components u_{kw} and T_{kw} are Fourier-transformed to frequency space where the spectral expansion coefficients
373 χ_{kw} in domains outside the desired frequency ranges are put to zero. Case (i) results in KW components $u_{kw,l}$ and $T_{kw,l}$ where
374 l indicates the low-frequency component. Case (ii) results in $u_{kw,m}$ and $T_{kw,m}$ where m indicates the intramonthly period.
375 Case (iii) results in fields $u_{kw,h}$ and $T_{kw,h}$ where h stands for the high-frequency component. Previous studies have defined
376 free propagating Kelvin waves over similar ranges (3-20 days, Alexander and Ortland (2010); 4-23 days, Suzuki and Shiotani
377 (2008)) and similarly for intraseasonal periods (23-92 days, Suzuki and Shiotani (2008)). Next, seasonal averages will be taken
378 over the four seasons, resulting in variables $\overline{u_{kw,l}}^s$, $\overline{T_{kw,l}}^s$ for the low-frequency component and similarly for the other two
379 cases. The superscript s represents one of the four seasons: northern winter ($s = DJF$), spring ($s = MAM$), summer ($s = JJA$),
380 and autumn ($s = SON$).

381 Cases (ii) and (iii) contain purely subseasonal variability and therefore one can expect their ~~mean 6-year~~ fields means to be
382 zero-valued since variability beyond 90 days has been put to zero. Similarly, mean fields for each of the four seasons results

383 in $\overline{u_{kw,h}}^s \ll \overline{u_{kw,l}}^s$ and $\overline{u_{kw,m}}^s \ll \overline{u_{kw,l}}^s$ and the same for the temperature component. This reflects the fact that positive
384 and negative phases of the fast KW responses average out to approximately zero on seasonal timescales (figure not shown).
385 Therefore, the seasonal mean ~~over-of~~ the absolute amplitudes ~~for-of-the~~ zonal wind and temperature are examined instead,
386 i.e. $|\overline{u_{kw,h}}^s|$, $|\overline{u_{kw,m}}^s|$ and similarly for temperature ~~component, in-order-to-study~~. This describes seasonal fluctuations in
387 subseasonal KW amplitudes³.

388 Figure 7 shows results for all three cases after taking mean over the whole period. The left panel resembles a dominant
389 "wave-1" structure with zonal wind maximized around 140 hPa. Easterly KW winds are strongest around 60°E and westerly
390 winds around the Date Line. Note that two stationary perturbations over African (30°E) and South American (80°W) orography
391 are the result of our terrain-following NMF analysis. If one compares the KW zonal wind pattern with the climatological zonal
392 wind pattern in Fig. 3(a) it can be observed that the zonal wind pattern is located around 20° west of the climatological pattern.
393 Wave temperature perturbations are largest where the vertical gradients in zonal wind are largest which explains the ~~quadripole~~
394 ~~structure. Heating (cooling) by KWs is quadrupole structure. Warm and cold KW anomalies are~~ located at 100 hPa in ~~Eastern~~
395 ~~(Western) Hemisphere and the other way around~~ the Eastern and Western hemisphere, respectively, and vice versa at 200-300
396 hPa.

397 The average low-frequency or seasonal KW structure has a significant resemblance with the classical Gill-type KW solution
398 (Gill, 1980) describing a steady-state linear wave response to convective forcing. The Gill-type KW solution is characterized
399 by westerly upper-troposphere winds east of the large-scale convective source. In responds to the seasonal cycle of convection,
400 the solution in Fig. 7a illustrates, in addition to a low-frequency KW variability in westerly winds, also a considerable
401 low-frequency variability west of the convective outflow. This part of the signal represents the wave modulation effect of
402 the propagating KWs on seasonal timescales.

403 The middle panel of Fig. 7 shows the average distribution of KW activity on intraseasonal timescales. The activity is largest
404 in the Eastern Hemisphere hemisphere with average zonal wind maxima up to 3 ms⁻¹ and temperature maxima up to 0.7 K.
405 Zonal wind activity is largest over a broad area between 90 and 150 hPa over the Indian Ocean and the Maritime Continent.
406 Temperature activity occurs slightly higher around 90-100 hPa. Intraseasonal activity is locally somewhat increased also around
407 120°W, west of the Andes mountain range.

408 Finally, Fig. 7c illustrates the average distribution of ~~free-propagating-intramonthly~~ KWs. The Eastern ~~Hemisphere~~ hemisphere
409 again makes up for the larger KW activity than the Western hemisphere, but the maximum is located more upward in compar-
410 ison to the intraseasonal scales, around 80 hPa. Zonal wind activity peaks up to 3 ms⁻¹ over a broad range of 70-110 hPa and
411 temperature peaks over a more narrow area around 76 hPa (up to 0.75 K). The main area for KW activity is found over Indian
412 Ocean region, while least wave activity is above central Pacific. Towards the stratosphere KW activity reduces and becomes
413 more uniform along in ~~longitudal~~ longitudinal direction.

³Most previous studies define KW activity as square amplitude rather than absolute amplitude. In our high resolution dataset we observe highly localized patterns of the KW activity in the Eastern hemisphere due to ongoing wave amplification. By using absolute amplitudes we better visualize the longitudinal structure of the KW activity in comparison to its local maxima.

414 4.2 Low-frequency Kelvin wave variability

415 The seasonal patterns of the low-frequency components of the KW (~~from hereon referred to as the Gill-type KW response~~) is
416 presented as pressure-longitudinal cross-sections along the equator (at 0.7°N) of the KW seasonal means, given by $\overline{[u_{kw,l}]^s}$
417 and $\overline{[T_{kw,l}]^s}$ in Fig. 8.

418 The largest ~~Gill-type KW response is found during NH summer~~ amplitudes are found during the JJA months. A strong dipole
419 "wave-1" pattern is evident in the TTL. The strongest zonal winds are found close to 150 hPa with easterlies up to -12 ms^{-1}
420 centered over Indian Ocean and westerlies up to 6 ms^{-1} over the Western Pacific. Negative temperature KW anomalies at 110
421 hPa are strongest as well during JJA with values up to 1.5 K over Indian Ocean and annually averaged value of -0.5 K over
422 Western Pacific.

423 During ~~NH winter DJF~~, the dipole pattern ~~is has~~ shifted more eastward and upward compared to ~~NH summer JJA~~ and has a
424 more slanted structure. Easterly (westerly) KW winds are located more east over the Maritime continent (central Pacific) and
425 are centered at 130 hPa. The upper temperature dipole pattern is found higher up at 90 hPa approximately. Values are somewhat
426 weaker compared to NH summer with easterlies up to -6 ms^{-1} and westerlies up to 5 ms^{-1} .

427 Finally, ~~NH autumn and spring seasons SON and MAM season months~~ are transition seasons with respect to the strength
428 and position of the KW dipole as it moves west- and downward towards ~~summer JJA~~ and east- and upward towards ~~winter NH~~
429 ~~spring DJF~~. MAM has the weakest KW dipole with slightly stronger westerly winds up to 5 ms^{-1} .

430 The longitudinal position and the strength of the ~~Gill-type low-frequency~~ KWs have been linked to the seasonal patterns of
431 the background winds in the TTL representing the upper level monsoon and Walker circulations (Flannaghan and Fueglistaler,
432 2013). The average background winds maximize at 150 hPa as shown in Fig. 3(a). In Fig. 8, one can see how the KW easterlies
433 in ~~Eastern Hemisphere the Eastern hemisphere~~ are strongest during ~~NH summer JJA~~ in relation to the Indian-South Asian
434 monsoon circulation. Background easterlies as strong as -30 ms^{-1} are located approximately 10° east of the KW maximum
435 easterlies. ~~NH winter DJF~~ has the strongest background westerlies in relation to the upper-level circulation of the Western
436 Pacific anticyclones. ~~NH spring (autumn) MAM~~ shows similar background wind patterns compared to ~~NH winter (summer)~~
437 DJF but with weaker circulation. SON shows similar patterns with JJA but with weaker winds.

438 Further details on longitudinal position and interannual variability of ~~Gill-type the low-frequency~~ KW response at its max-
439 imum value at 150 hPa are illustrated by the Hovmoller diagram in Fig. 9. For comparison, tropical convection is represented
440 as well through the OLR proxy variable averaged over 15°S - 15°N latitudes. All fields have been filtered with a 90 day cut-
441 off low-pass filter in order to highlight the seasonality. As a result, one can observe enhanced/reduced ~~Gill-type~~ KW activity
442 during the same individual seasons as seen from the timeseries in Fig. 5. Above average seasonal KW activity with stronger
443 Gill-type dipole structures occurred during the summer of 2007 (mainly through its easterlies at 60°E) and during the winters
444 of 2006-2007 and 2009-2010. In these winters, El-Nino was active and a clear longitudinal eastward shift is observed in OLR,
445 in the background circulation (not shown), as well as in the Gill-type dipole KW structure. The El-Nino winter of 2009-2010
446 was followed by a strong La Nina winter with an increase in tropical convection over the Maritime continent (note: OLR values
447 below 195 Wm^{-2}).

448 The vertical seasonal movement of the KW dipole has been linked with the seasonal movement of the tropical tropopause
 449 height (Flannaghan and Fueglistaler, 2013; Ryu et al., 2008). The position of the tropical tropopause height (represented by
 450 a static stability value of $5 \times 10^{-4} \text{ s}^{-2}$ in Fig. 8) is found at approximately 85 hPa during winter-DJF and descends towards
 451 100 hPa in summer-JJA, similar to values obtained from GPS-RO observations by Grise et al. (2010). In particular, during
 452 summer-JJA, one can notice how the asymmetry in the tropical tropopause height over Indian Ocean around 60°E coincides
 453 with increasing temperatures by the KW dipole up to 1.5 K. Such deformation of the tropical tropopause is also evident during
 454 winter and autumn-DJF and SON seasons.

455 Figures 10a and 10b illustrate seasonal-mean KW temperatures $\overline{T_{kw,l}}^s$ in relation to the tropical tropopause layer defined by
 456 static stability N^2 . Seasonal variations in KW temperatures are collocated with the position of the tropopause, descending down
 457 from its highest position during winter-DJF to its lowest position during summer-JJA. Temperature amplitudes are observed to
 458 decline roughly above $N^2 = 5 - 6 \times 10^{-4} \text{ s}^{-2}$. Within this zonal-mean seasonal picture, zonal asymmetries in N^2 exist and are
 459 found: (i) near the Date Line with values of $8 \times 10^{-4} \text{ s}^{-2}$ at 80 hPa during winter-DJF and $7 \times 10^{-4} \text{ s}^{-2}$ at 90 hPa during summer
 460 JJA and (ii) lower at 100 hPa over the Indian Ocean during summer-JJA. Particularly during NH-summer-JJA, the deformation
 461 of the zonal-mean static stability field collocates strongly with the position of a strong KW temperature anomaly over Indian
 462 Ocean. A rough estimation is made on the contribution of the KW anomaly to the zonal deformation of the tropopause layer by
 463 removing zonal-mean parts of both fields. First, static stability zonal anomalies, $\overline{N'^2}^s$, are derived by subtracting zonal-mean
 464 values of N^2 from the full N^2 field per timestep and at every pressure level, followed by seasonal averaging. Next, we can
 465 estimate the static stability change associated with the KW anomaly, using the relation: $N_{kw}^2 = \frac{g}{\theta} \frac{\partial \theta_{kw}}{\partial z}$, followed by seasonal
 466 averaging as well, i.e. $\overline{N_{kw}^2}^s$.

467 As a result, Fig. 10c and 10d show how both static stability anomalies are overlapping. During winter-DJF, the structure of
 468 the zonal anomaly $\overline{N'^2}^s$ has a positively-valued tilt eastward which stretches up to 80 hPa, while during summer-JJA a strong
 469 static stability anomaly is found more localized over Indian ocean region with values in the TTL up to $\overline{N'^2}^{JJA} = \pm 0.8 \times 10^{-4}$
 470 s^{-2} . The anomaly associated with the KW temperature anomaly is found to peak up to $+0.6 \times 10^{-4} \text{ s}^{-2}$ during summer-JJA
 471 and up to $+0.4 \times 10^{-4} \text{ s}^{-2}$ during winter-DJF. Finally, by dividing both fields with each other, the resulting contribution of the
 472 quasi-stationary Kelvin wave to the observed deformation of the tropical tropopause layer is estimated up to 60% (during JJA
 473 and 80%)-during-NH-summer-(winter)during DJF.

474 4.3 Intraseasonal Kelvin wave variability

475 The seasonality of intraseasonal Kelvin wave variability is shown in Fig. 11 and shall be briefly discussed here. The NH-winter
 476 DJF stands out as the most active season for KW activity, located mainly in the Eastern hemisphere centered-centred at 100°E
 477 and with maximum activity at 110 hPa for zonal wind and temperature with a second maximum in temperature at 90 hPa.
 478 Values observed are up to 0.8 K for KW temperature and 5 ms^{-1} for KW zonal wind. During NH-spring-MAM season, the
 479 KW activity fields are weaker but spread over a larger area in the Eastern hemisphere and in the TTL with maximum activity
 480 centered at 120 hPa (90 hPa) for the zonal wind (temperature) component. Both NH-summer and autumn-JJA and SON seasons
 481 have KW activity positioned at lower altitudes and more westward. In both seasons, KW zonal wind activity is split up between

482 two structures with an eastward tilt with height; one with a maximum around 110°E and one pattern starting from 100 hPa and
483 extending towards 60°E. Note also the increase in KW activity in the Western hemisphere below 150 hPa in the East Pacific.
484 The maximum KW activity in the temperature component for both seasons is positioned near 100 hPa approximately on the
485 tropical tropopause contour with value $5 \times 10^{-4} \text{ s}^{-2}$.

486 The eastward tilted structure is observed throughout all seasons except ~~NH-spring~~ ~~MAM~~ when background easterly winds
487 are nearly absent in the Eastern hemisphere. In all other seasons one can observe how the tilted structure is locked to the
488 background easterlies with maximum amplitudes located slightly above and west of it. Such eastward tilt with height has
489 been frequently observed, for example over radiosonde station Medan at 100°E during the early stage of MJO development
490 (Kiladis et al., 2005).

491 **4.4 Intramonthly Kelvin waves**

492 **4.5 Free-propagating Kelvin-waves**

493 The seasonal variability of ~~free-traveling~~ ~~intramonthly~~ Kelvin waves, represented by their absolute amplitudes $\overline{|u'_{kw,h}|^2}$ and
494 $\overline{|T'_{kw,h}|^2}$, shall be examined in relation to the background conditions. Figure 12 illustrates favorable regions for KW activity. In
495 general, KW activity increases upward from around 120 hPa towards its zonal-mean peak value at 76 hPa. The largest values
496 are observed in ~~EH~~ ~~the Eastern hemisphere~~ in region from 30°E till 150°E. The temperature component in particular has a
497 constant maximum peak (up to 0.8 K in ~~EH~~) located around 76 hPa throughout the year, where also the largest increase in N^2
498 occurs as shown in Fig. 3. Above 70 hPa, KW activity continuously decreases in the stratosphere.

499 The longitudinal structure of the KW zonal wind shows two distinct peaks in the TTL, one consistently located at 76
500 hPa and another around 100-110 hPa in the ~~EH~~ ~~Eastern hemisphere~~ which is mainly present during solstice seasons. The
501 first maximum coincides with the temperature distribution which can be explained by their balance relationships and free
502 horizontal propagation in the stratosphere. Below the tropopause, KW activity is coupled to convective processes alternating
503 the tropospheric vertical wave structures as discussed by Flannaghan and Fueglistaler (2012).

504 The secondary maximum around 110 hPa in Fig. 12 is present mainly during solstice seasons in ~~EH~~ ~~the Eastern hemisphere~~
505 and it is associated with the seasonal movement of the background wind. The maximum of KW wind and the background wind
506 maximum move eastward from ~~winter-to-summer~~ ~~DJF to JJA~~ season similar to the low-frequency variability. A day-by-day
507 comparison of the KW activity and background wind confirms that propagating KWs amplify while approaching a region of
508 strong easterlies, forming a folding structure around it while the individual KWs dissipate towards the center of easterly winds.
509 One can notice in Fig. 12 a fast reduction of KW amplitudes eastward of its maximum towards the center of the background
510 easterlies. It is likely related to dissipation and wave breaking processes as observed over Indonesia (120°E) by Fujiwara et al.
511 (2003). Within such regions, the KW-background wind interaction becomes complex and the linearity assumption breaks
512 (Ryu et al., 2008; Flannaghan and Fueglistaler, 2013).

513 A comparison with the previous study by Suzuki and Shiotani (2008) using ERA-40 data shows that the L91 data contain
514 stronger KW activity in the vicinity of the background easterlies in the Eastern ~~Hemisphere~~ ~~hemisphere~~, and more fine-scale

515 details which can be explained by better analyses based on more observations and improved models including increased
516 resolution. For example, Suzuki and Shiotani (2008) used 5 levels of ERA-40 data between 50 and 200 hPa whereas the present
517 study considers 25 model levels between 50 – 200 hPa. Maxima of the KW temperature signal appear in similar locations and
518 strength except for a small offset in vertical position (70 hPa in Suzuki and Shiotani (2008) versus 80 hPa in Fig. 12) and a
519 larger zonal asymmetry in our results.

520 Another view of the seasonal cycle of free propagating KWs is illustrated in Fig. 13 which focuses on the spatiotemporal
521 distribution of individual KW ~~packetstracks~~. Hovmoller diagrams ~~are illustrated~~ of KW zonal wind and temperature at levels
522 110 and 200 hPa ~~cumulated~~ from different years ~~are shown into a single calendar year~~ along with the background zonal wind.
523 In addition, the monthly-mean values of daily maximum KW amplitudes occurring ~~at a specific longitude along the equator are~~
524 ~~added next to in longitude are added on the rightside of~~ each diagram. ~~It represents seasonality in the KW maximum amplitudes~~
525 ~~in a similar fashion to Fig. 6 in Alexander and Ortland (2010) which is based on HIRDLS satellite data.~~

526 The individual wave tracks at 110 hPa illustrate KWs with amplitudes exceeding 3 ms^{-1} and 0.6 K which are propagating
527 throughout the year in the Eastern ~~Hemisphere~~~~hemisphere~~, during June–October months only over the Pacific, and all except
528 ~~winter-DJF~~ months in most of the Western Hemisphere. Typical wave tracks start east of the 0° (30°W) meridian during
529 winter (summer) and largely disappear west of 120°E . The largest wave amplitudes are observed between 50°E and 100°E
530 prior to regions of easterly winds in agreement with Fig. 12. Here presented details show that most notable waves appear
531 during the Asian monsoon period with upper-level easterlies prevailing from June into September. The largest ~~Kelvin-wave~~
532 ~~KW~~ amplitudes appear confined to the June and July months followed by a rapid drop in August. In fact, a local minimum in
533 the number of KWs as well as in wave amplitudes occurs in August before the KW activity increases slightly during autumn.

534 At 200 hPa, the favorable area for KW propagation shifts to the Western Hemisphere and large KW activity is observed
535 west of the South American continent throughout the year (west of 80°W) with a westward extension over the Pacific during
536 ~~northern-summer~~~~JJA~~. Another set of wave tracks starts over ~~equatorial~~~~equatorial~~ South America around 30°W (5°W) and
537 continues till 60°E (~~during JJA. During DJF these wave tracks shift more east and start at 5°W and continue till 90°E) during~~
538 ~~northern-summer (winter)~~. The seasonal shifts of approximately 30° in KW tracks collocate with similar shifts in the prevailing
539 TTL winds.

540 The amplitude of KWs undergoes a clear annual cycle with a small secondary peak present during ~~northern-winter~~~~DJF~~, as
541 represented by the monthly-means of daily maximum amplitudes ~~along the equator~~ on the rightside of Fig. 13. The largest
542 amplitudes are found at 110 hPa during ~~NH-summer~~~~JJA~~ with monthly-mean zonal wind (temperature) values up to 8.5 ms^{-1}
543 (1.8 K) in June. During the ~~winter-DJF~~ months Kelvin waves amplify more eastward with monthly-mean zonal wind (temper-
544 ature) values up to 7.8 ms^{-1} (1.6 K) in December. ~~Our result matches well with the observed seasonal pattern in maximum~~
545 ~~KW temperatures at 16km ($\sim 100 \text{ hPa}$) from the HIRDLS satellite observations (Alexander and Ortland, 2010, Fig. 6).~~ At 200
546 hPa, KW amplitudes are on average lower with a yearly-averaged amplitude reduction around 55% in temperature and 35% in
547 zonal wind.

548 The semiannual cycle in maximum amplitudes remains visible up till 70 hPa. Above 70 hPa, where the KW activity remains
549 large in Eastern ~~Hemisphere~~ hemisphere (Fig. 12), the semiannual cycle is replaced by an interannual cycle in line with the
550 dominant impact of the QBO.

551 **5 Discussion and Conclusions**

552 We have applied the multivariate decomposition of the ECMWF operational analyses during the period 2007-2013 when
553 the operational data assimilation ~~was and forecasting were~~ performed on 91 ~~levels. Model-level data were analyzed every 6~~
554 ~~hours. The applied model levels. The applied normal-mode function~~ decomposition provides simultaneously the wind com-
555 ponents, geopotential height and temperature perturbations of ~~the Kelvin waves on the terrain-following levels~~ Kelvin waves
556 for many scale without any prior data filtering. The three-dimensional Kelvin wave structure in the upper troposphere and
557 lower stratosphere is composed of Kelvin wave solutions of 60 linearized shallow-water equation systems on the sphere with
558 equivalent depths from 10 km up to about 3 meters. As the KW meridional wind component is very small it is not discussed -
559 here. We showed that large-scale KWs readily persist in the data despite analyzing selected processing times independently.

560 The KW is a normal mode of the global atmosphere and our 3D-orthogonal decomposition allows quantification of its
561 contribution to the global energy spectrum and variability. We have presented the total (kinetic+potential) energy of KWs in
562 the L91 data as a function of the zonal wavenumber in different seasons. The zonal wavenumber $k = 1$ contains the largest
563 portion of KW energy in all seasons. There is almost one third more energy in JJA than in MAM in $k = 1$. In $k = 2$ there is
564 50% less energy than in $k = 1$ but JJA still contains most energy. In all larger zonal wavenumbers, the most energetic season is
565 DJF.

566 We focused on the spatiotemporal features of the KW temperature and zonal wind components in the four seasons. The
567 Kelvin wave seasonal cycle in the tropical tropopause layer (TTL) was compared with seasonal variability of the Outgoing
568 Longwave Radiation (OLR), and the background wind and stability fields, which are believed to play an important role for
569 the KW variability. Our study results of the seasonal KW variability ~~complements complement~~ previous studies which applied
570 different methods for the KW filtering and different datasets. ~~As KW is a normal mode of the global atmosphere, our filtering~~
571 ~~of the KW using the 3D-orthogonal normal-mode function decomposition of global data is a useful approach to quantification~~
572 ~~of the KW variance. The KW is the most energetic inertio-gravity mode of the global atmosphere (Žagar et al., 2009) and~~
573 ~~its representation in weather and climate models is crucial for reliable simulations of the tropics and its impact on global~~
574 ~~circulation.~~

575 ~~We have presented the total energy of the KWs in the L91 data extending between the surface and 1 Pa as a function of the~~
576 ~~zonal wavenumber. Zonal wavenumber $k = 1$ contains a largest portion of KW energy in all seasons. Its energy varies between~~
577 ~~~ 300 in JJA in NH spring to over 400 J/kg in NH summer. In $k = 2$ there is 50% less energy than in $k = 1$ but the NH summer~~
578 ~~is still the most energetic season. In all greater zonal wavenumbers, DJF season contains most energy.~~

579 Frequency The frequency spectrum has revealed a semiannual cycle as well as intraseasonal and intramonthly variabil-
580 ity. Three ranges of wave periods were analyzed: 3-20 days, 20-90 days and longer than 90 days. This choice was partly

581 deliberate in order to compare our results with several previous studies of KW variability. First we demonstrated that the
582 ~~seasonal-mean KW low-frequency KW dipole~~ pattern in the TTL, with ~~(westerly-) easterly-westerly~~ winds in the ~~(Western-)~~
583 ~~Eastern hemisphere resembles a time-averaged Western hemisphere and with easterly winds in the Eastern hemisphere, partly~~
584 ~~resembles a seasonal-averaged~~ Gill-type "wave-1" pattern ~~and contains partly low-frequency modulation of vertically-propagating~~
585 ~~KWs~~. The quadrature-shaped temperature component represents a thermally adjusted pattern with respect to the zonal wind
586 component, and contributes to seasonal ~~(cooling)-warming~~ above 100 hPa in the ~~(Eastern) Western Western and cooling in the~~
587 ~~Eastern~~ hemisphere. The largest KW amplitudes are observed during ~~summer and winter JJA and DJF~~ seasons. From boreal
588 summer towards winter, KW ~~perturbation-perturbations~~ moves eastward (from Indian Ocean basin towards Maritime Conti-
589 nent) and upward (e.g. zonal wind component moves up from 150 hPa towards 120 hPa). The KW zonal wind amplitude varies
590 between 12 m/s strong easterlies over Indian ocean near 150 hPa in JJA to 6 m/s over Western Pacific. Over Indian Ocean in
591 JJA, the KW easterlies thus make almost half of the total wind vector. The associated KW temperature perturbations are from
592 1.5 K over Indian ocean in JJA to -0.5 K over West Pacific. The zonal modulation of Kelvin waves is found to be locked with
593 respect to the seasonal movement of convection and the convective outflow in the TTL. The modulation effect is strongest
594 for ~~Gill-type the low-frequency~~ Kelvin waves during the summer monsoon season, when strong easterly winds are present at
595 150 hPa, resulting in the largest KW zonal wind and temperature anomalies, of which the latter results in deformation of the
596 tropical tropopause over Indian Ocean.

597 Intraseasonal (periods 20-90 days) activity is strongest in ~~NH-winter DJF~~ with maxima up to 0.8 K for KW temperature
598 and up to 5 m/s for KW zonal wind centred at 120°E. Both temperature and zonal wind activities have eastward tilt with
599 height. In comparison to previous study by Suzuki and Shiotani (2008) using ERA-40 data, the slanted structure in the present
600 data continues to extend more upward and eastward which is likely due to the increased number of vertical model levels
601 compared to ERA-40. The importance of vertical model resolution for the KW ~~wave~~-structure and amplitude was demonstrated
602 in Žagar et al. (2012) and Podglajen et al. (2014).

603 For periods 3–20 days, the seasonal cycle of KWs is clearly seen in ~~the~~ wave amplitude. ~~The In the zonal-mean perspective,~~
604 ~~the~~ largest amplitudes are located ~~-from a zonal-mean perspective-~~ between 70 and 100 hPa for both zonal wind and tem-
605 perature ~~as expected for the free-propagating Kelvin waves~~ but it is modulated by the seasonal movement of the TTL. A
606 major zonal asymmetry was found in KW activity: around 110 hPa ~~the~~ Kelvin wave undergoes amplification mainly in ~~Eastern~~
607 ~~Hemisphere the Eastern hemisphere~~ during the solstice seasons, while at 200 hPa a secondary region of ~~the~~ KW amplifica-
608 tion occurs in ~~Western Hemisphere the Western hemisphere~~ during boreal summer. ~~Free-propagating The intermonthly~~ KWs
609 show largest amplitudes in the vicinity of the strongest easterlies preferably west and above the ~~center-centre~~ of easterlies. The
610 ~~NMF methodology has made applied novel methodology makes~~ it possible to observe such dynamics on daily basis whenever
611 easterlies are strong in the TTL. Nearly real-time representation of the KW activity is available on <http://modes.fmf.uni-lj.si>.

612 In summary, our seasonal variability analysis shows that the background wind in the TTL linked with convective outflows,
613 play a dominant role in the longitudinal position where ~~the~~ zonal modulation of Kelvin waves is preferred, while the tropical
614 tropopause and its seasonal vertical movement ~~determines-determine~~ the vertical extent of ~~the~~ KW modulation processes.

615 *Acknowledgements.* This study was funded by the European Research Council (ERC), Grant Agreement no. 280153 [MODES](http://meteo.fmf.uni-lj.si/MODES), <http://meteo.fmf.uni-lj.si/MODES>.
616 [MODES](#). We are grateful to Dr George Kiladis and an anonymous reviewer for their detailed constructive comments.

617 **References**

- 618 Alexander, M. J. and Ortland, D. A.: Equatorial waves in High Resolution Dynamics Limb Sounder (HIRDLS) data, *J. Geophys. Res.*, 115,
619 D24 111, <https://doi.org/10.1029/2010JD014782>, 2010.
- 620 Andrews, D. G., Holton, J. R., and Leovy, C. B.: *Middle atmospheric dynamics*, Academic Press, 1987.
- 621 Baldwin, M. P. and Coauthors: The Quasi-Biennial Oscillation, *Rev. Geophys.*, 39, 179–229, 2001.
- 622 Boyd, J. P.: The Effects of Latitudinal Shear on Equatorial Waves. Part II: Applications to the Atmosphere, *J. Atmos. Sci.*, 35, 2259–2267,
623 1978.
- 624 Boyd, J. P.: *Dynamics of the Equatorial Ocean*, Springer-Verlag GmbH Germany 2018, 2018.
- 625 Boyd, J. P. and Zhou, C.: Uniform Asymptotics for the Linear Kelvin Wave in Spherical Geometry, *J. Atmos. Sci.*, 65, 655–660,
626 <https://doi.org/10.1175/2007JAS2356.1>, 2008.
- 627 Ern, M. and Preusse, P.: Wave fluxes of equatorial Kelvin waves and QBO zonal wind forcing derived from SABER and ECMWF temperature
628 space-time spectra, *Atmos. Chem. Phys.*, 9, 3957–3986, 2009.
- 629 Ern, M., Preusse, P., Krebsbach, M., Mlynczak, M. G., and Russell, J. M.: Equatorial wave analysis from SABER and ECMWF temperatures,
630 *Atmos. Chem. Phys.*, 8, 845–869, 2008.
- 631 Flannaghan, T. J. and Fueglistaler, S.: Tracking Kelvin waves from the equatorial troposphere into the stratosphere, *J. Geophys. Res.*, 117,
632 <https://doi.org/10.1029/2012JD017448>, d21108, 2012.
- 633 Flannaghan, T. J. and Fueglistaler, S.: The importance of the tropical tropopause layer for equatorial Kelvin wave propagation, *J. Geophys.*
634 *Res.*, 118, 5160–5175, 2013.
- 635 Fueglistaler, S., Dessler, A. E., Dunkerton, T. J., Folkins, I., Fu, Q., and Mote, P. W.: Tropical tropopause layer, *Reviews of Geophysics*, 47,
636 <https://doi.org/10.1029/2008RG000267>, 2009.
- 637 Fujiwara, M., Yamamoto, M. K., Hashiguchi, H., and Horinouchi, T.: Turbulence at the tropopause due to breaking Kelvin waves observed
638 by the Equatorial Atmosphere Radar, *Geophysical Research Letters*, 30, 1171, <https://doi.org/10.1029/2002GL016278>, 2003.
- 639 Garcia, R. R. and Salby, M. L.: Transient response to localized episodic heating in the Tropics. Part II: Far-field behavior, *J. Atmos. Sci.*, 44,
640 499–530, 1987.
- 641 Garcia, R. R., Lieberman, R., Russell III, J. M., and Mlynczak, M. G.: Large-scale waves in the mesosphere and lower thermosphere observed
642 by SABER, *J. Atmos. Sci.*, 62, 4384–4399, <https://doi.org/10.1175/JAS3612.1>, 2005.
- 643 Gill, A. E.: Some simple solution for heat-induced tropical circulation, *Quart. J. Roy. Meteor. Soc.*, 106, 447–462, 1980.
- 644 Gill, A. E.: *Atmosphere-Ocean Dynamics*, Academic Press, New York, 1982.
- 645 Grise, K. M., Thompson, D. W. J., and Birner, T.: A global survey of static stability in the stratosphere and upper troposphere, *J. Climate*, 23,
646 2275–2292, 2010.
- 647 Hayashi, Y.: Space-time spectral analysis and its applications to atmospheric waves, *J. Meteor. Soc. Japan*, 60, 156–171, 1982.
- 648 Highwood, E. J. and Hoskins, B. J.: The tropical tropopause, *Q.J.R. Meteorol. Soc.*, 124, 1579–1604, 1998.
- 649 Holton, J. R.: *An introduction to dynamical meteorology*, vol. 4, Elsevier Academic Press, 2004.
- 650 Holton, J. R. and Lindzen, R. S.: An updated theory for the quasi-biennial cycle of the tropical stratosphere, *J. Atmos. Sci.*, 29, 1076–1080,
651 1972.
- 652 Kasahara, A.: Normal modes of ultralong waves in the atmosphere, *Mon. Wea. Rev.*, 104, 669–690, 1976.

653 Kasahara, A.: Effect of zonal flows on the free oscillations of a barotropic atmosphere, *J. Atmos. Sci.*, 37, 917–929. Corrigendum, *J. Atmos.*
654 *Sci.*, 38 (1981), 2284–2285, 1980.

655 Kasahara, A. and Puri, K.: Spectral representation of three-dimensional global data by expansion in normal mode functions, *Mon. Wea. Rev.*,
656 109, 37–51, 1981.

657 Kedzierski, R. P., Matthes, K., and Bumke, K.: The tropical tropopause inversion layer: variability and modulation by equatorial waves,
658 *Atmos. Chem. Phys.*, 16, 11 617–11 633, <https://doi.org/10.5194/acp-16-11617-2016>, 2016.

659 Kiladis, G. N., Straub, K. H., and Haertel, P. T.: Zonal and vertical structure of the Madden–Julian Oscillation, *J. Atmos. Sci.*, 62, 2790–2809,
660 <https://doi.org/10.1175/JAS3520.1>, 2005.

661 Liebmann, B. and Smith, C. A.: Description of a complete (interpolated) outgoing longwave radiation dataset, *Bull. Am. Meteorol. Soc.*, 77,
662 1275–1277, 1996.

663 Lin, J.-L. and Coauthors: Tropical intraseasonal variability in 14 IPCC AR4 climate models. Part I: Convective signals, *J. Climate*, 19,
664 2665–2690, 2006.

665 Matsuno, T.: Quasi-geostrophic motions in the equatorial area, *J. Meteor. Soc. Japan.*, 44, 25–43, 1966.

666 Podglajen, A., Hertzog, A., Plougonven, R., and Žagar, N.: Assessment of the accuracy of (re)analyses in the equatorial lower stratosphere,
667 *J. Geophys. Res. Atmos.*, 119, 11 166–11 188, <https://doi.org/10.1002/2014JD021849>, 2014.

668 Randel, W. J. and Wu, F.: Kelvin wave variability near the equatorial tropopause observed in GPS radio occultation measurements, *J.*
669 *Geophys. Res.*, 105(D12), 15 509–15 523, <https://doi.org/10.1029/2000JD900155>, 2005.

670 Ratnam, M. V., Tsuda, T., Kozu, T., and Mori, S.: Long-term behavior of the Kelvin waves revealed by CHAMP/GPS RO measurements and
671 their effects on the tropopause structure, *Ann. Geophys.*, 24, 1355–1366, 2006.

672 Ryu, J.-H., Lee, S., and Son, S.-W.: Vertically propagating Kelvin Waves and tropical tropopause variability, *J. Atmos. Sci.*, 65, 1817–1837,
673 2008.

674 Salby, M. L. and Garcia, R. R.: Transient response to localized episodic heating in the tropics. Part I: Excitation and short-time near-field
675 behavior, *J. Atmos. Sci.*, 44, 458–498, 1987.

676 Shumway, R. and Stoffer, D.: Time series analysis and its applications: with R examples, Springer texts in statistics, Springer New York,
677 <https://doi.org/https://books.google.si/books?id=dbS5IQ8P5gYC>, 2010.

678 Son, S.-W., Lim, Y., Yoo, C., Hendon, H. H., and Kim, J.: Stratospheric Control of the Madden–Julian Oscillation, *Journal of Climate*, 30,
679 1909–1922, <https://doi.org/10.1175/JCLI-D-16-0620.1>, 2017.

680 Suzuki, J. and Shiotani, M.: Space-time variability of equatorial Kelvin waves and intraseasonal oscillations around the tropical tropopause,
681 *J. Geophys. Res.*, 113, D16 110, <https://doi.org/10.1029/2007JD009456>, 2008.

682 Tindall, J. C., Thuburn, J., and Highwood, E. J.: Equatorial waves in the lower stratosphere. II: Annual and interannual variability, *Q.J.R.*
683 *Meteorol. Soc.*, 132, 195–212, <https://doi.org/10.1256/qj.04.153>, 2006.

684 Tsai, H.-F., Tsuda, T., Hajj, G., Wickert, J., and Aoyama, Y.: Equatorial Kelvin waves observed with GPS occultation measurements (CHAMP
685 and SAC-C), *J. Meteor. Soc. Japan.*, 82, 397–406, 2004.

686 Žagar, N., Andersson, E., and Fisher, M.: Balanced tropical data assimilation based on a study of equatorial waves in ECMWF short-range
687 forecast errors, *Q.J.R. Meteorol. Soc.*, 131, 987–1011, <https://doi.org/10.1256/qj.04.54>, 2005.

688 Žagar, N., Andersson, E., Fisher, M., and Untch, A.: Influence of the quasi-biennial oscillation on the ECMWF model short-range forecast
689 errors in the tropical stratosphere, *Q. J. R. Meteorol. Soc.*, 133, 1843–1853, 2007.

690 Žagar, N., Tribbia, J., Anderson, J. L., and Raeder, K.: Uncertainties of estimates of inertia-gravity energy in the atmosphere. Part II: Large-
691 scale equatorial waves, *Mon. Wea. Rev.*, 137, 3858–3873, Corrigendum: 138:2476–2477, 2009.

692 Žagar, N., Terasaki, K., and Tanaka, H. L.: Impact of the vertical resolution of analysis data on the estimates of large-scale inertio-gravity
693 energy, *Mon. Wea. Rev.*, 140, 2297–2307, 2012.

694 Žagar, N., Kasahara, A., Terasaki, K., Tribbia, J., and Tanaka, H.: Normal-mode function representation of global 3D datasets: Open-access
695 software for the atmospheric research community, *Geosci. Model Dev.*, 8, 1169–1195, 2015.

696 Wallace, J. M. and Gutzwiller, V. E.: Observational evidence of Kelvin waves in the tropical stratosphere, *J. Atmos. Sci.*, 25, 900–907, 1968.

697 Wheeler, M. and Kiladis, G. N.: Convectively coupled equatorial waves: Analysis of clouds and temperature in the wavenumber-frequency
698 domain, *J. Atmos. Sci.*, 56, 374–399, 1999.

699 Yang, G.-Y. and Hoskins, B. J.: ENSO impact on Kelvin Waves and associated tropical convection, *J. Atmos. Sci.*, 70, 3513–3532, 2013.

700 Yang, G.-Y., Hoskins, B. J., and Slingo, J.: Convectively coupled equatorial waves: A new methodology for identifying wave structures in
701 observational data, *J. Atmos. Sci.*, 60, 1637–1654, 2003.